New Particle Formation in the Tropical Free Troposphere during CAMP²Ex: Statistics and Impact of Emission Sources, Convective ~~activity~~Activity, and Synoptic Condition

Qian Xiao[1], Jiaoshi Zhang[1], Yang Wang[2], Luke D. Ziemba[3], Ewan Crosbie[3,4], Edward L. Winstead[3], Claire E. Robinson[3], Joshua P. DiGangi[3], Glenn S. Diskin[3], Jeffrey S. Reid[5], K. Sebastian Schmidt[6], Armin Sorooshian[7,8], Miguel Ricardo A. Hilario[8], Sarah Woods[9], Paul Lawson[9], Snorre A. Stamnes[3], Jian Wang[1]

[1]Department of Energy, Environmental and Chemical Engineering, Washington University in St. Louis, St. Louis, MO 63130, USA
[2]Department of Chemical, Environmental and Materials Engineering, University of Miami, Coral Gables, FL 33124, USA
[3]NASA Langley Research Center, Hampton, VA 23666, USA
[4]Science Systems and Applications, Inc., Hampton, VA 23666, USA
[5]Marine Meteorology Division, Naval Research Laboratory, Monterey, CA, USA
[6]Laboratory for Atmospheric and Space Physics, University of Colorado, Boulder, CO 80309, USA
[7]Department of Chemical and Environmental Engineering, University of Arizona, Tucson, AZ, 85721, USA
[8]Department of Hydrology and Atmospheric Sciences, University of Arizona, Tucson, AZ 85721, USA
[9]Stratton Park Engineering Company (SPEC), Boulder, CO 80301, USA

Correspondence to: Jian Wang (jian@wustl.edu)

Abstract. Nucleation in the free troposphere (FT) and subsequent growth of new particles represents a globally important source of cloud condensation nuclei (CCN). Whereas new particle formation (NPF) has been shown to occur frequently in the upper troposphere over tropical oceans, there have been few studies of NPF at lower altitudes over the tropical marine environment. In addition, the impact of anthropogenic emissions and biomass burning on NPF over the tropics remains poorly understood. In this study, we examine NPF in the lower and mid troposphere (3-8.5 km) over ocean and coastal regions of the Sulu Sea and Northern Subtropical Pacific Ocean in Southeast Asia using airborne measurements during the recent Cloud, Aerosol and Monsoon Processes Philippines Experiment (CAMP²Ex). CAMP²Ex took place from 25 August through 5 October 2019, including both late southwest monsoon and monsoon transition. Recent NPF events, as evidenced by elevated concentrations of newly formed particles (i.e., particles of diameters between 3 and 10 nm), were observed during 4% of the total flight time (5 out of 128 hours). The frequency of NPF increases with altitude, reaching 49% above an altitude of 8 km. NPF was mostly observed at altitudes above ~~3~~5 km and coincided with elevated relative humidity (RH), suggesting that NPF is closely associated with convective cloud outflow in conditions of low temperature and reduced ~~pre-existing particle concentrations~~condensation sink (CS). Air masses are categorized into background, biomass burning-influenced, and urban-influenced air based on in-situ CO, CH_4 and O_3 measurements. NPF in background air was mostly observed above 6 km, typically accompanied by the lowest ~~surface area~~CS among all air mass types. NPF occurred above the 0 ºC level at 5.5-7 km in air masses influenced by convectively detrained biomass burning and/or urban emissions and was enhanced by 1) scavenged primary particles; 2) elevated precursor concentrations and 3)

enhanced irradiance due to cloud reflections. However, NPF was suppressed in aged urban influenced air masses where the reactive precursors were mostly consumed while existing particle surface area remained relatively high due to longer aerosol lifetimes in the free troposphere. The results highlight the role of convective clouds that efficiently scavenge existing aerosol particles, inject reactive precursors into free troposphere, and enhance UV irradiance, all of which facilitate NPF. This study also illustrates the competing influences of different variables and complex interactions between anthropogenic emissions, transport, convective clouds, and meteorology, which lead to NPF under a variety of conditions and at different altitudes in tropical marine environment.

1 Introduction

New particle formation (NPF), the process of gas to particle nucleation and early growth to 2-3 nm, has been observed in many regions and over a wide range of altitudes, i.e., from the pristine to heavily polluted environment, from the tropics to the Arctic, and from boundary layer (BL) to tropopause layer (TL) (Chae et al., 2011; Twohy et al., 2002; Dada et al., 2017; Andreae et al., 2018; Kerminen et al., 2018; Zheng et al., 2021; Reid et al., 2016). Modelling studies suggest that on a global average NPF contributes up to approximately half of the cloud condensation nuclei (CCN) in the troposphere (Gordon et al., 2017), and strongly influences cloud formation and climate (Kulmala et al., 2014). The rate of NPF depends on the concentrations of low volatility vapors (e.g., H_2SO_4 and highly oxygenated organics) that participate in the NPF, and the rate is also a function of temperature. As these low volatility vapors are mostly formed by photochemistry, their concentrations depend on the intensity of solar radiation as well as the concentration of precursors. Essentially all long-term surface measurements show that the average solar radiation intensity is stronger during NPF event days compared with non-event days. Pre-existing aerosol particles serve as both a condensational sink for the low volatility vapors and a coagulation sink for newly formed particles, therefore they are expected to inhibit NPF. Indeed, observations at many locations have shown that new particle events in the troposphere typically occur under clean conditions (Kerminen et al., 2018; Kuang et al., 2009).

Over the oceans, NPF is typically observed in the free troposphere (FT). It had been long thought that NPF rarely occurs within the remote marine boundary layer, because primary sea spray aerosols (SSA) present large condensation and coagulation sinks (Pirjola et al., 2000). A recent study shows that NPF takes place regularly in the upper part of the decoupled marine boundary layer following the passage of cold fronts over mid-latitude ocean, due to the combination of low existing aerosol loading, cold temperature, availability of reactive gases, and high actinic fluxes in the clear regions between scattered cumulus clouds (Zheng et al., 2021). In boundary layer over coastal regions, NPF can occur in continental outflow such as transported urban plumes (Reid et al., 2016). In the FT over tropical and mid-latitude oceans, NPF was mostly observed in the air mass processed by convective clouds (Clarke et al., 1998; Clarke et al., 1999; Perry and Hobbs, 1994; Williamson et al., 2019). Intense NPF in convective outflow regions was observed in the tropical upper troposphere over both Pacific and Atlantic oceans (Williamson et al., 2019). Chemical-transport model simulations indicate this NPF in the tropical upper troposphere is a globally important source of CCN in the lower troposphere. In the outflow of convective clouds, existing particles are

depleted due to wet scavenging, leading to low condensation and coagulation sinks that promote NPF. At the same time, reactive gases such as dimethyl sulfide (DMS) are transported from marine boundary layer to the outflow region, where the actinic flux is high and the reactive gases react to form low volatility species that participate in NPF (Williamson et al., 2019). Concurrent observations of elevated H_2SO_4 vapor concentration with the newly formed particles over the open ocean suggest that H_2SO_4 formed from oxidation of DMS likely plays an important role in NPF. While NH_3 and highly oxygenated compounds (HOM) can participate in NPF, modeling studies have shown that between 5.8 km altitude and the top of the troposphere, on average globally, about 80% of NPF at these altitudes involves only sulfuric acid and water (binary nucleation; Gordon et al., 2017), and a large fraction of the NPF is ion-induced, especially over oceans where the overall NPF rate is relatively low (Dunne et al., 2016; Gordon et al., 2017). In addition to cloud outflow regions, newly formed particles were also observed in the FT near the edge of cumulus clouds with enhanced actinic flux (Wehner et al., 2015), and in continental outflow just above the boundary layer cloud top (i.e., lower FT) over the northwestern Atlantic (Corral et al., 2022) and northeastern Pacific (Dadashazar et al., 2018).

Previous studies have greatly advanced our understanding of NPF in the marine environment. Over tropical oceans, most studies focused on the NPF in the upper troposphere (UT), whereas the observations of NPF in the outflow of convective clouds in the middle FT (i.e., 4-8 km) remain scarce (Clarke et al., 1998; Williamson et al., 2019). ~~Model simulation from the perspective of galactic cosmic rays suggests~~Kirkby et al. (2011) found that ion-induced binary nucleation associated with galactic cosmic ray ~~aerosol formation in the lower and middle troposphere is weak~~can occur in the mid FT but is negligible in the boundary layer, while the strongest aerosol formation takes place in upper troposphere over tropic oceans (Kazil et al., 2006). In addition, previous measurements were mostly carried out in pristine environments. As a result, the impact of anthropogenic emissions on NPF over tropical oceans is still poorly understood. In this study, we take advantage of comprehensive airborne measurements during the Cloud, Aerosol and Monsoon Processes Philippines Experiment (CAMP²Ex) to investigate NPF from the lower (~3 km) to upper FT (~8.5 km) in both background air masses and those impacted by urban emissions and biomass burning. The monsoon transition was captured during CAMP²Ex, allowing us to examine the impact of both changing air mass origins and convective activity on NPF. Through both statistical analysis and case studies, we quantify the frequency of NPF and the conditions under which NPF occurs in different air masses and their dependence on altitude. These results help improve the understanding of NPF in tropical marine environments, both in background conditions and under the influence from anthropogenic emissions.

2 Methodology

2.1 Measurements Onboard the Aircraft

The Cloud, Aerosol and Monsoon Processes Philippines Experiment (CAMP²Ex), with the objective of characterizing the role of anthropogenic and natural aerosols in aerosol-cloud interaction in the vicinity of Philippines, included deployments onboard both the NASA P-3B aircraft and SPEC Learjet 35A (Reid et al.,

2023)~~(Reid et al., submitted)~~. The data analyzed in this study are all from the NASA P-3B aircraft, which flew 19 research flights (flight tracks were superimposed on map as shown in Fig. S1) from 24 August to 5 October 2019, covering South China Sea (SCS), Sulu Sea, West Pacific, and the continental FT. The CAMP^{2}Ex campaign provided an excellent dataset to investigate NPF from the lower to upper troposphere (3-8.5 km) in a range of air masses, including background air and those influenced by Borneo biomass burning smoke, Asian pollution, and local emissions from Philippines (Hilario et al., 2021).

The measurements examined in this study include aerosol properties, carbon monoxide (CO), methane (CH$_4$) and ozone (O$_3$) mixing ratios, meteorological parameters, and radiation (see Table 1 for details). Three condensation particle counters (CPCs, Model 3756 and 3772, TSI Inc.; Hermann et al., 2007) measured the total number concentrations of particles nominally larger than ~3 and ~10 nm ($N_{>3\ nm}$ and $N_{>10\ nm}$) as well as non-volatile particle concentration ($N_{>10nm,non-volatile}$), respectively. Aerosol size distributions were characterized by a fast integrated mobility spectrometer (FIMS, 10-600 nm; Wang et al., 2017a; Wang et al., 2017b; Wang et al., 2018) and a laser aerosol spectrometer (LAS, Model 3340, TSI Inc., 100-3000 nm). The cloud droplet spectra were measured by a fast cloud droplet probe (FCDP, SPEC Inc.; Lawson et al., 2017). Several trace gases measured in-situ onboard the P-3B are used to identify different air mass origins. CO and CH$_4$ mixing ratios were characterized by a dried-airstream near-infrared cavity ring-down absorption spectrometer (Model G2401-m, PICARRO Inc.; Digangi et al., 2021; Baier et al., 2020). O$_3$ was measured by a dual-beam UV adsorption sensor (Model 205; 2B Technologies; Digangi et al., 2021). Water vapor mixing ratio and relative humidity (RH) were given by a diode laser hygrometer at 1 Hz (DLH; Diskin et al., 2002; Podolske et al., 2003). Upwelling and downwelling shortwave irradiance from 350-2150 nm were measured by the solar spectral flux radiometer (SSFR; Norgren et al., 2022; Schmidt et al., 2021; Chen et al., 2021).

Table 1. **Information on instruments involved in NPF analysis.**

Parameter/Variable	Instruments/Methods	Sampling frequency
Aerosol number concentration (> 3 nm)	Condensation particle counter (CPC, TSI-3756)	1 Hz
Aerosol number concentration (> 10 nm)	Condensation particle counter (CPC, TSI-3772)	1 Hz
Number concentration of non-volatile particles (> 10 nm)	Condensation particle counter (CPC, TSI-3772) downstream of a thermodenuder	1 Hz
Aerosol size distribution (10-600 nm)	Fast integrated mobility spectrometer (FIMS)	1 Hz
Aerosol size distribution (100-3000 nm)	Laser aerosol spectrometer (LAS, TSI-3340)	1 Hz
Cloud droplet size distribution (2-50 μm)	Fast cloud droplet probe (FCDP, SPEC Inc.)	1 Hz

Ozone mixing ratio	Dual cell broadband UV absorption spectrometry (2B Technologies, Model 205)	0.4 Hz
CO and methane mixing ratio (dry mass fraction)	Near-IR cavity ringdown absorption spectroscopy (PICARRO Inc., G2401-M)	0.4 Hz
Relative humidity with respect to water (RH)	Diode laser hygrometer (DLH, NASA Langley Research Center)	1 Hz
Upwelling and downwelling shortwave irradiance	Solar spectral flux spectrometer (SSFR)	1 Hz
Latitude/longitude/GPS altitude	Litton 251	1 Hz
Air temperature	Rosemont 102 Fast	1 Hz

130

When P-3B was inside clouds, aerosol measurements were impacted by shattering of cloud droplets and/or ice particles on the iso-kinetic aerosol sampling inlet. The in-cloud periods and additional 3-second buffer time immediately before and after in-cloud periods were identified based on hydrometeor measurements (i.e., cloud flag, available in CAMP[2]Ex data archive https://asdc.larc.nasa.gov/project/CAMP2Ex). Aerosol measurements during the

135   flagged periods were excluded from the analysis to minimize the influence of the measurement artifacts. Condensation sink (CS) reflects how quickly condensable vapors will condense on the existing aerosol (Dal Maso et al., 2002). We calculated CS from the ambient aerosol size distribution (Kulmala et al. 2012), which was derived by combining dry particle size distribution measured by FIMS (10-600 nm) and LAS (600-1000 nm), ambient RH, and an average hygroscopicity parameter (κ). Aerosol mass spectrometer (AMS) measurements show that on average,

140     $(NH_4)_2SO_4$ represents 90% of the PM_1 mass above 5 km, where vast majority of the NPF events was identified. A κ value of 0.53 was therefore applied to calculate particle hygroscopic growth factor at ambient RH (Petters and Kreidenweis, 2007) for each size bin of the combined dry size distribution. Total aerosol surface area concentration was derived from the combined size distribution from multiple instruments, including FIMS and LAS, which collectively cover the size range of 10-3000 nm. All aerosol number concentrations (number and surface area)

145   concentrations and size distributions are reported at standard temperature and pressure (1013.25 hPa and 273.15 K, STP). As there was no direct measurement of actinic flux, which reflects the intensity of photo-oxidations, we calculated the ultraviolet (UV) irradiance by integrating the measured irradiance over the wavelength range of 350-400 nm from the SSFR and used it as a proxy. The total UV irradiances were derived as the sum of both upwelling and downwelling components. Examining both upwelling and downwelling components also provides insights into

150   the factors that influence the total UV irradiance and thus photochemistry during the NPF periods.

2.2 Identification of NPF Events

Ideally, the concentration of incipient particles (i.e., particles with diameter around 1.5 nm) should be used to identify new particle formation (NPF) events. However, given the challenges of measuring incipient particle concentration at below 2 nm onboard the research aircraft, many airborne studies have used the ratio of concentration ratio of the particles with diameter above 3 nm ($N_{>3\ nm}$) to that above 10 nm ($N_{>10\ nm}$) and/or the number concentration of particles between 3 nm and 10 nm (N_{3-10nm}) to characterize NPF events (Crumeyrolle et al., 2010; Zheng et al., 2021). In this study, we used $N_{>3\ nm}/N_{>10\ nm}$ ~~the~~ to identify NPF events, following a similar approach described by Zheng et al. (2021).. A ratio ($N_{>3\ nm}/N_{>10\ nm}$) substantially above 1 indicates the presence of newly formed particles between 3 and 10 nm, and thus a recent NPF event. Considering the response times of the CPCs to step changes in particle concentration (i.e., about 2 seconds to reach 90% of concentration step change), we first averaged the 1-second measurements of particle number concentrations (i.e., $N_{>3\ nm}$ and $N_{>10\ nm}$) into 10-s intervals. For each of the 10-s intervals, the ratio of average $N_{>3\ nm}$ to average $N_{>10\ nm}$ and the uncertainty of the ratio (σ_R) were derived. New particles are considered to be present when the ratio is above 1.3 plus three times uncertainty as an assumed noise floor:

$$\frac{N_{>3\ nm}}{N_{>10\ nm}} > 1.3 + 3 \cdot \sigma_R \qquad (1)$$

An NPF event was identified when at least three consecutive 10-s intervals indicate the presence of newly formed particles. Given the P3 flew at ~160 m/s, this translates into a minimum spatial scale of ~5 km. In total 105 NPF events were identified, and the durations range from 30 to 1150 s, corresponding to spatial scales of 5-196 km.

To contrast the conditions between NPF events and non-NPF events, we also defined non-NPF periods following a similar approach. Specifically, a non-NPF period consists of a minimum of 6 consecutive 10-s intervals (i.e., a minimum of 60 s in duration) with all intervals during the period showing the ratio of averaged particle concentrations (i.e., $N_{>3\ nm}/N_{>10\ nm}$) statistically below 1.05:

$$\frac{N_{>3\ nm}}{N_{>10\ nm}} < 1.05 - 3 \cdot \sigma_R \qquad (2)$$

We note the criteria for non-NPF periods is quite strict. Due to measurement counting statistics, some of the non-NPF periods might not be identified even though no newly formed particles are present. Similarly, some weak new particle events might not be picked up by the criteria (i.e., Eq. (1)) described above either.

2.3 K-means Classification

To examine the conditions that lead to NPF, we performed k-means clustering on the matrix consisting of event mean values of ~~aerosol surface area concentration~~CS, RH, ~~air~~ ambient temperature, and UV irradiance for 95 NPF events (10 events are excluded due to missing data for one or more of the four variables). RH was included as one of the variables because an elevated RH in the mid to upper FT often indicates air with more moisture and reactive

gases (e.g., DMS) that are vertically transported by convective clouds from the lower atmosphere (Reid et al., 2019). The transported reactive gases can be subsequently oxidized to form low volatility species that participate in NPF (Ahern et al., 2019). In addition, elevated water vapor/RH in the cloud outflow regions is typically associated with high concentration of water vapor, which has been shown to participate in binary nucleation (Vehkamäki et al., 2002). The total UV irradiance (i.e., the sum of both upwelling and downwelling components) was included as a proxy for actinic flux due to the absence of direct measurement.

The four variables (e.g., RH, ~~aerosol particle surface area concentration~~CS, a~~mbient~~~~ir~~ temperature, and UV irradiance) were first normalized using z-score standardization. The optimal number of clusters K was determined as six using the elbow method together with Silhouette coefficient (Syakur et al., 2018; Rousseeuw, 1987). We then performed the k-means clustering via MATLAB based on k-means ++ algorithm (Arthur and Vassilvitskii, 2007; Lloyd, 1982) and a prescribed setting of 5,000 iterations. Consequently, the 95 NPF events were clustered into 6 groups, and each contained 7-35 NPF events. General statistics of six clusters in terms of four key variables are presented in Table 2.

~~Table 2. Mean general statistics of key parameters for the 6 clusters identified using k-means classification.~~

~~Cluster #~~	~~Number of events~~	~~Total duration, s~~	~~Mean altitude, m~~	~~Mean temperature, °C~~	~~Mean UV irradiance, W m⁻²~~	~~Mean RH, %~~	~~Mean surface area, μm² cm⁻³~~
~~1~~	~~25~~	~~4910~~	~~7587.6~~	~~-14.6~~	~~106.1~~	~~76.3~~	~~4.1~~
~~2~~	~~14~~	~~4320~~	~~6480.8~~	~~-8.8~~	~~60.8~~	~~81.9~~	~~2.6~~
~~3~~	~~30~~	~~4590~~	~~5944.6~~	~~-4.4~~	~~108.0~~	~~77.1~~	~~2.9~~
~~4~~	~~8~~	~~1010~~	~~7568.2~~	~~-14.0~~	~~119.6~~	~~30.6~~	~~4.7~~
~~5~~	~~12~~	~~890~~	~~6727.5~~	~~-10.3~~	~~95.6~~	~~62.0~~	~~15.6~~
~~6~~	~~6~~	~~400~~	~~3959.3~~	~~4.2~~	~~58.1~~	~~74.2~~	~~9.5~~

Table 2. General statistics of key parameters for the 6 clusters identified using k-means classification.

Cluster #	Number of events	Amount of 1-s data	Mean±std altitude, m	Mean±std temperature, °C	Mean±std UV irradiance, W m⁻²	Mean±std RH, %	Mean±std CS, 10^{-3} s⁻¹
1	35	5550	6104.6±591.9	-4.6±3.3	108.8±13.6	75.4±9.0	1.1±0.5
2	20	3870	7708.8±433.2	-15.2±2.4	104.5±13.1	79.8±8.5	2.0±0.7
3	13	3960	6392.4±369.8	-7.3±1.8	60.9±14.4	82.6±7.0	1.1±0.5
4	9	1190	7532.1±438.2	-12.9±2.5	118.8±21.2	33.3±13.5	1.2±0.6
5	11	790	6698.5±650.7	-10.3±4.2	93.7±23.6	61.3±6.3	5.1±1.2
6	7	400	3959.3±671.3	4.2±4.3	58.1±24.1	74.2±10.5	2.9±2.0

2.4 Development of Chemical Influence Flag

To investigate the impact of air mass type on NPF, we classified air masses sampled during CAMP²Ex into three types ~~following a similar approach by DiGangi et al (in preparation, also in CAMP²Ex Archive)~~ (the details of the approach can be found at: https://doi.org/10.5067/Airborne/CAMP2Ex_TraceGas_AircraftInSitu_P3_Data_1). The flag partitions sources by the observed ratios of enhancement in methane to that in CO ($\Delta CH_4/\Delta CO$) through a combination of absolute and correlative methods into 4 regimes: background air (background, hereafter), biomass burning (BB-influenced, hereafter), air mass influenced by urban (urban-influenced, hereafter) and mixed urban/biomass burning. The classification is largely based on $\Delta CH_4/\Delta CO$, taking advantage of the relatively long lifetime of both trace gases in the FT. Here the term background is defined to differentiate air masses from the other two types (i.e., impacted by biomass burning or urban emission), which does not strictly refer to very clean conditions. As reported by literature (Nara et al., 2017; Worden et al., 2017), low $\Delta CH_4/\Delta CO$ has been frequently observed in biomass burning plumes (typically < 10%), whereas much higher ratios (typically close to 100%) have been reported in fossil fuel combustion emissions (Helfter et al., 2016). In this study, we use ~~these~~ the first three regimes to investigate the impact of air masses on NPF by focusing on NPF events observed in background, biomass burning and urban-influenced air masses.

3 Overview of NPF Events during CAMP²Ex ~~Overall Statistical Analysis~~

3.1 General Statistics

~~There was a total of 19 research flights (RFs) during CAMP²Ex. These RFs covered the ocean east and west of Luzon Island, and two of them (RF8 and RF18) sampled over Luzon Island and upwind/downwind of Metro Manila. The date and sampling area of all RFs, together with the duration and key variables of observed NPF events, are presented in Table S1. Most NPF events were observed above 3 km when RH exceeded 50%, and only about 2% of total NPF was observed at 3.5-5 km. A few events were identified within the boundary layer about 50 kilometers downwind west of metro Manila, which are closely associated with shipping and/or urban emissions. These NPF events likely occurred immediately following the dilution of vehicle and engine emissions (e.g., Uhrner et al., 2011; Wehner et al., 2009), and they are not included in further analyses. The number concentration of newly formed particles ($N_{3\text{-}10\text{ nm}}$) above 3 km shows large variations among different research flights. NPF frequency, defined as the ratio of the sampling time when new particles were observed to the total flight time, decreased drastically starting from RF11 on 19 September and no events were observed from RF12 through RF17 as shown in Fig. 1. This sudden decrease in NPF frequency coincided with the early monsoon transition starting on 20 September (Hilario et al., 2021). The impact of the southwest monsoon phase on the occurrence of NPF will be discussed in Sect. 3.3.~~

There was a total of 19 research flights (RFs) during CAMP²Ex. Figure 1 shows an overview of the flight tracks and the locations where NPF in three major air mass types was observed. These RFs covered the ocean east and west of

Luzon Island, and two of them (RF8 and RF18) sampled over Luzon Island and upwind/downwind of Metro Manila. The date and sampling areas of all RFs, together with the duration and key variables of observed NPF events, are presented in Table S1. Most NPF events were observed above 5 km when RH exceeded 50%. A few short periods with elevated $N_{>3\ nm}/N_{>10\ nm}$ (not counted as NPF events) were observed within the boundary layer about 50 kilometers downwind west of metro Manila during RF18, which are closely associated with shipping and/or urban emissions. These NPF events likely occurred immediately following the dilution of vehicle and engine emissions (e.g., Uhrner et al., 2011; Wehner et al., 2009), and they are not included in further analyses. NPF frequency, defined as the ratio of the sampling time when new particles were observed to the total flight time, decreased drastically starting from RF11 on 19 September and no events were observed from RF12 through RF17 as shown in Fig. S1. This sudden decrease in NPF frequency coincided with the early monsoon transition starting on 20 September (Hilario et al., 2021).
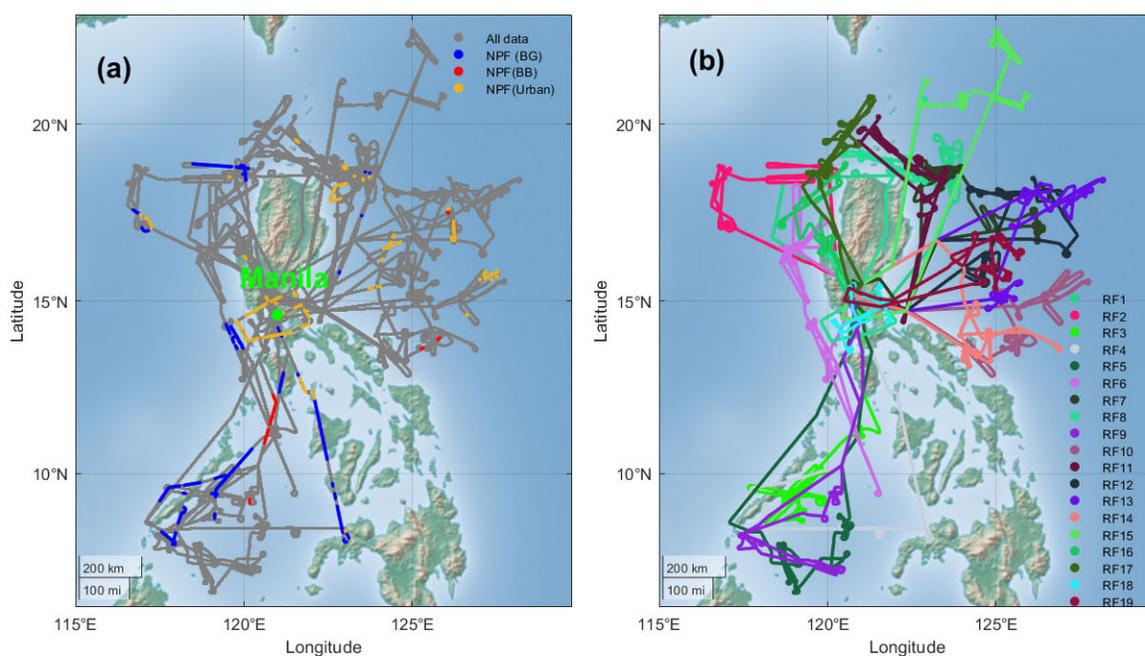
~~Figure 1. Amount of data sampled during each RF (bars) and corresponding NPF frequency (orange dots), which is defined as the ratio of the duration of NPF events to the total sampling time during the flight.~~

Figure 1. (a) NPF events during the whole mission color coded by three air mass types (NPF events occurred in mixed regimes are not shown here). (b) Locations of 19 flight tracks.

3.2 Dependence of NPF Frequency on Air Mass Types

One objective of this study is to investigate the features of NPF and the influence of emission sources on NPF at different altitudes. For each of the three air mass types (i.e., background, urban-influenced, and BB-influenced), NPF frequency is calculated for each 500 m altitude bin. Figure S2 shows the vertical profiles of CS for three air

mass types. Background air masses have lowest CS on average below 4 km and above 6 km (except for 7-7.5 km) among all three air mass types, whereas BB-influenced air masses have the highest CS at lower altitudes (i.e., < 4 km) and urban-influenced air masses dominates the higher altitudes (> 6 km). The condensation sinks of three air mass types are comparable in between. In addition, we compare the vertical profiles of the existing surface areaCS and RH between NPF and non-NPF periods, i.e., periods when newly formed particles were observed and absent, respectively (see Sect. 2.2 for the definitions of NPF and non-NPF periods). Note that due to the limited sampling, no non-NPF periods above 7.5 km are identified based on the criteria described in Sect. 2.2. For the comparison above 7.5 km, the non-NPF period is instead defined as the entire period when P3-B sampled outside of clouds except when newly formed particles were observed (i.e., when Eq. (1) is satisfied).

Figure 2a shows that below 5.5 km, no NPF events were observed in background or BB-influenced air masses and NPF frequency is very low (below 3%) and NPF was mostly observed in the air influenced by urban emissionsurban-influenced air masses. No NPF events were observed in BB-influenced and only minor events took place in the background air masses at ~3.5 km. NPF frequency shows strong increases with altitude above 6 km for all three air mass types, reaching about 49% above 8 km. Figure 2c 2b shows that over the entire altitude ranges examined, NPF consistently occurred in air with elevated RH. This suggests NPF in outflow regions and detrainment layers of convective clouds, which is confirmed by the flight video, is also consistent with earlier studies (Clarke et al., 1998; Perry and Hobbs, 1994). Previous studies show that the mixing of air mass with different temperature and precursor concentrations can lead to enhanced nucleation rates (Khosrawi and Konopka, 2003; Nilsson and Kulmala, 1998; Nilsson et al., 2001; Wehner et al., 2010). In the outflow regions, the mixing of cloud outflow and surround air may also contribute to the observed NPF events. Figure 2c shows that most NPF events occurred when CS was below 0.002 s^{-1}. For NPF events observed above 6.5 km, the median CS value is mostly below ~ 0.001 s^{-1}, comparable to the CS below 8 × 10^{-4} s^{-1} globally in the tropical mid-FT reported by Williamson et al. (2019). However, the impact of surface areaCS on NPF shows an altitude dependence (Fig. 2b2c). Above 5.5 km, newly formed particles were observed when surface area was reduced,with reduced CS, generally consistent with the higher NPF frequency in background air mass. In contrast, NPF coincided with relatively high surface areaCS below 5.5 km, where all most NPF events were observed in urban influenced air masses. The altitude dependence of the impact relationships amongof air masses, and surface areaCS on and NPF implies the competing influences from different processes (i.e., production and removal of nucleating species) that variesvary with altitude, which will be further discussed in Sect. 4. We also compare the NPF frequency, CS and RH as a function of altitude between SWM and MT periods (see Fig. S3). The NPF frequency during the MT is lower than that during SWM at most altitudes above 5 km. The decrease of NPF frequency during the MT is due to, at least partially, closely related tothe higher CS and lower RH, which may be is likely attributed to thea result of reduced convective activity and thus reduced wet scavengingaltered meteorological conditions. The more frequent long range transport of aged urban plumes may also contribute to the elevated CS during the MT (Hilario et al., 2021).
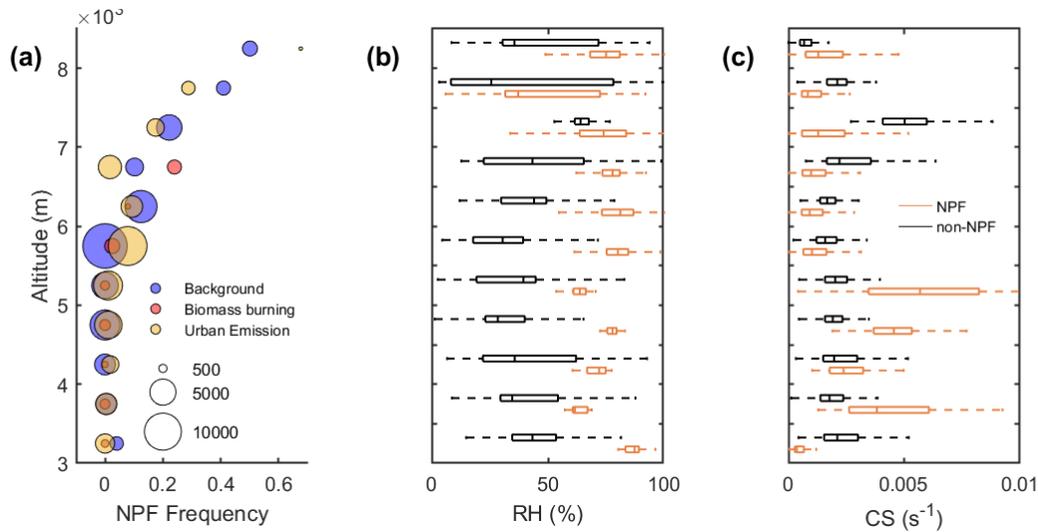
Figure 2. (a) The vertical profile of NPF frequency for the three air mass types. NPF Frequency is defined as the ratio of total duration of NPF period to the total sampling time outside of the clouds for each airmass type. Also shown are the comparison of (b) RH and (c) ~~relative humidity (RH)~~CS between NPF and non-NPF periods, where black denotes non-NPF and orange denotes NPF.

~~**3.3 Impact of Monsoon Transition on NPF Frequency**~~

~~As shown in Fig. 1, the NPF frequency during the southwest monsoon (SWM; RF1-11) with its Maritime Continent source region was much higher than that during the Monsoon transition/post monsoon phase (MT; RF12-19). The reduction of NPF frequency occurs at all altitudes above 5.5 km during the MT. The RH was higher during SWM compared to that during MT over most altitudes above 3 km (Fig. 3c), whereas the surface area was generally lower during SWM (Fig. 3b). These differences suggest that lower NPF frequency during the MT is due to, at least partially, the higher surface area (larger condensation and coagulation sinks), which is likely a result of less convective activity and thus reduced precipitation that would remove existing particles. The more frequent long-range transport of aged pollution from East Asia may also contribute to the higher surface area during the MT (Hilario et al., 2021).~~
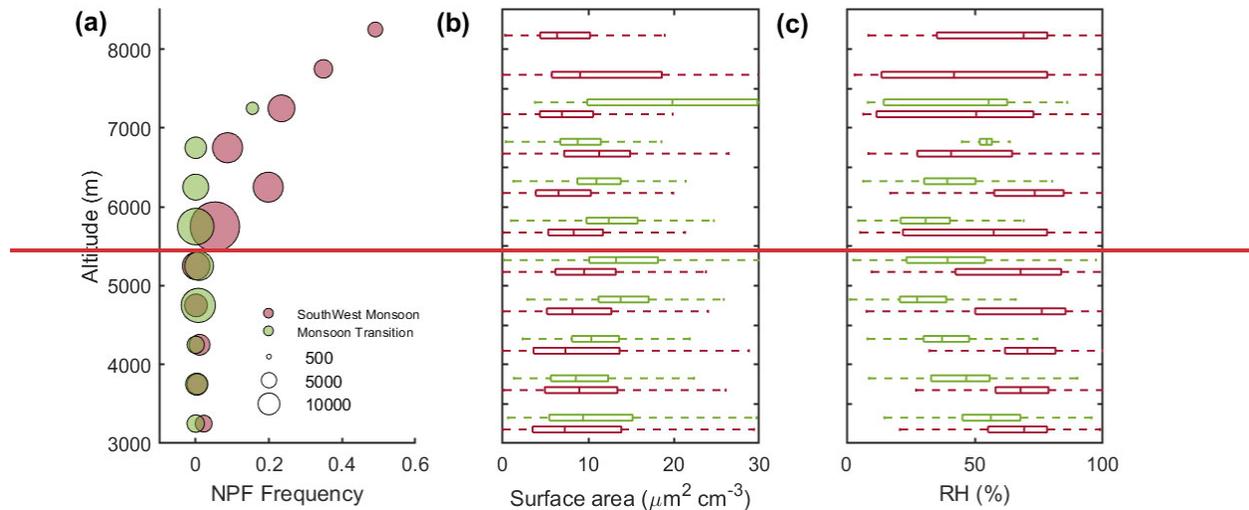
3.~~3~~4 K-means Classification Results

As described in Sect. 2, a total number of 95 NPF events were classified into six clusters based on RH, temperature, UV irradiance and ~~surface area~~CS. Figure 4~~3~~ shows the contributions of air mass types to each cluster as well as the statistical comparison of key variables during NPF events of each cluster ~~and those during corresponding non-NPF~~ ~~events. For each NPF event cluster, the corresponding non-NPF events are defined as the periods when no newly~~ ~~formed particles were observed based on Eq. (2) within the same altitude range of the NPF events. This is to~~ ~~minimize the impact of altitude, as the NPF frequency strongly depends on the altitude (Fig. 2a).~~

Figure 4a ~~3a~~ shows the contribution of different air mass types to each NPF event cluster and the mean altitudes for the clusters. Clusters #1-3 represent the vast majority (i.e., 76%) of data collected during the NPF events. ~~e~~Cluster #~~3~~1 consists mostly of NPF events associated with polluted air masses (i.e., BB-influenced or urban-influenced). In contrast, NPF events in cluster #~~1~~2 and #~~2~~3 were mostly observed in background air, with a small portion in ~~in~~ ~~urban-influenced~~polluted air masses. ~~In contrast, cluster #3 consists mostly of polluted air masses (i.e., BB-~~ ~~influenced or urban-influenced).~~ Altogether, clusters #4-6 represent 24% of the NPF event data, the majority of which was observed in urban-influenced air masses. Figure 4~~b~~3b-f show that new particles form under a wide range of conditions, and the formation exhibits varying intensities, as suggested by different $N_{3-10\ nm}$ values in Fig. 3e. Most of the NPF events were observed in air masses with ~~surface area below 10 µm²·cm⁻³~~CS lower than 0.002 s⁻¹, ~~in~~ ~~good agreement~~comparable to ~~the~~ ~~with~~findings from earlier studies (Williamson et al., 2019)~~(Clarke et al., 1999)~~. ~~However, NPF events in cluster #5 occurred when SA was elevated compared to that during non-NPF periods at~~ ~~similar altitudes. These~~The NPF events ~~included in~~classified as cluster #5 have the highest CS compared to the other clusters and ~~-~~were mostly observed during RF18 and RF19~~, and part of this cluster corresponds to the NPF events~~

~~with higher surface area below 5.5 km shown in Fig. 2b.~~ ~~Part of cluster #5 corresponds to the NPF events with higher surface area below 5.5 km shown in Fig. 2b.~~ Both flights took place near the end of CAMP²Ex during monsoon transition, when air mass origins and meteorological conditions are likely different from those of earlier flights. The potential mechanism for such high CS NPF events will be discussed in Sect. 4.3. Figure ~~4b~~ 3b shows that most of NPF occurred with high actinic flux (indicated indirectly by the UV irradiance data during this campaign), as in clusters #1, #3, and ~~5~~#4. However, cluster #2 NPF events occurred with much lower UV irradiance level and ~~surface area~~CS, which will be discussed later in Sect. 4.1. In terms of RH, except for cluster #4, all NPF clusters were observed with median RH above 50% and the RH is statistically higher than that during corresponding non-NPF events (not shown), again indicating that NPF mostly takes place in air masses processed by convective clouds. NPF in cluster #4 occurred under the driest conditions (Fig. ~~4f~~3f) but with the highest UV irradiance (Fig. ~~4b~~3b), and $N_{3\text{-}10\ nm}$ is statistically the lowest among all clusters (Fig. ~~4e~~3e).

Because it takes some time for incipient particles to grow into the 3-10 nm size range, the NPF events identified here using $N_{>3nm}/N_{>10nm}$ value are likely several hours after the formation of the new incipient particles, depending on the actual growth rate. As the incipient particles are efficiently removed by coagulation inside clouds, we expect that air masses with elevated $N_{>3nm}/N_{>10nm}$ remained cloud free and did not experience precipitation since the recent particle formation. Therefore, CS and RH, which are among the NPF related parameters examined in this study, are unlikely to vary drastically over a period of several hours following the particle formation. New particle formation and subsequent particle growth can lead to an increase of CS. For elevated $N_{>3nm}/N_{>10nm}$ observed under conditions of low CS, the formation of new particles likely have occurred with comparable or even lower CS. UV irradiance has a strong diurnal variation and depends on the cloud condition, and it can change substantially over a period of several hours. In this study, most NPF events (i.e., elevated $N_{>3nm}/N_{>10nm}$) were observed at noontime under higher levels of UV irradiance compared to the non-NPF periods at the same altitude, consistent with earlier studies (Kerminen et al., 2018) showing that solar radiation was generally higher than during NPF event days compared with non-event days. This suggests that growth of new particles into the 3-10 nm size range during CAMP²Ex likely occurred over relatively short periods with no drastic changes in the UV irradiance. Some of the NPF events were observed under conditions of low UV irradiance, and the potential mechanisms are discussed in Sect. 4.1.
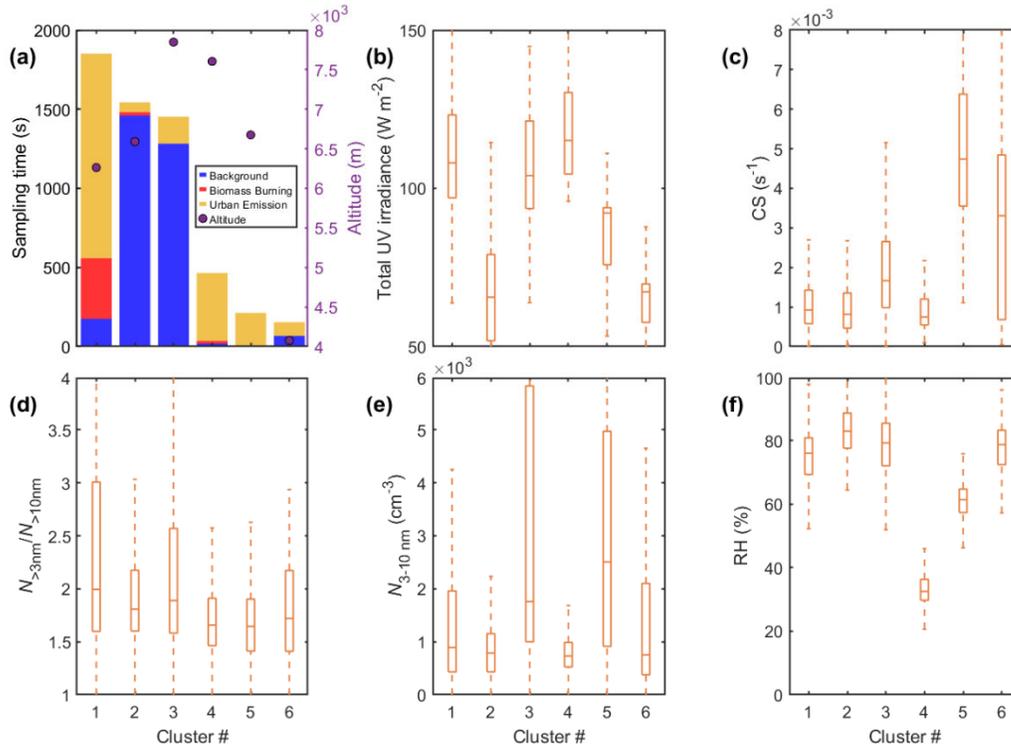
Figure 4~~3~~. (a) Number of 1-s data classified into each cluster and contributions of different air mass types. The other five panels compare ~~NPF events of each cluster and corresponding non-NPF periods at the same altitude ranges~~the clusters in terms of (b) total UV irradiance, (c) CS, (d) the ratio of number concentration of particle larger than 3 nm to that of particle larger than 10 nm~~,~~ ($N_{>3\ nm}/N_{>10\ nm}$), (e) number concentration of particles in diameter range of 3-10 nm~~,~~ ($N_{3-10\ nm}$) and~~,~~ (f) RH.

4 Characteristics of NPF in Different Air Mass Types

Here, we combine the k-means classification (i.e., based on T, RH, ~~surface area concentration~~CS and UV irradiance) and air mass classification to investigate the impact of both meteorological conditions and emissions on NPF. We divide the above clusters into multiple types, including NPF in background, mid-altitude NPF in polluted air, high-altitude NPF in polluted air, etc. In the following sections, we will examine NPF of each type and investigate the conditions that lead to NPF for different air masses as a function of altitude.

4.1 NPF Observed in Background Air

NPF in background air (CO concentration < 110 ppbv and CH_4 concentration < 1.86 ppm) was mostly observed in the early part of the campaign (i.e., RF2-RF6) during the southwest monsoon phase. These NPF events, mostly

classified as clusters #~~1~~ 2 and #~~2~~ 3 (Fig. ~~4a~~3a), took place from 6 km up to 8.5 km over Sulu Sea/West Luzon. General features of these events (background NPF, hereafter) are high RH and low ~~surface area~~CS, indicating new particles were formed in air processed by convective clouds.

We further divided background NPF events into two types based on the result of k-means classification: one classified into cluster #~~1~~ 2 ~~(mostly sampled during RF4 and RF6)~~ while the other classified into cluster #~~2~~3 (mostly sampled during RF4 and RF6). The main differences between these types include UV irradiance ~~(Fig. 5b)~~, ~~altitude~~temperature ~~(Fig. 5c)~~, and ~~surface area~~CS ~~(Fig. 5d)~~. Figure ~~5~~ 4 compares two types of background NPF in terms of ~~data number distribution as well as key statistics~~multiple variables as a function of RH. For both types, RHs are mostly in the range of 60-100% and concentrated between 70% and 90%. The high RH indicates that both types of NPF took place in cloud processed air (e.g., outflow region or detrainment layers). UV irradiance, $N_{>3\ nm}/N_{>10\ nm}$, and $N_{3\text{-}10\ nm}$ show similar variations with RH (Fig.~~5b~~4b, e, and f), and exhibit the highest values in the RH range of 60-80 %. This suggests UV irradiance plays an important role in these background NPF events, in agreement with the earliest findings of ~~Perry and Hobbs (1994)~~Perry and Hobbs (1994). The enhanced irradiance is attributed to the presence of clouds, as confirmed from the recorded videos by the forward camera onboard the P-3B. The effect of UV irradiance on NPF is also consistent with an earlier study (Wehner et al., 2015) that shows newly formed particles in regions with enhanced UV irradiance near cumulus clouds. The UV irradiance decreases from the peak values as RH increases above 80% and approaches 100%, accompanied by decreases in $N_{>3\ nm}/N_{>10\ nm}$ and $N_{3\text{-}10\ nm}$. The decrease in UV irradiance above 80% RH is likely due to attenuation of solar radiation in the immediate vicinity of clouds and between cloud layers (Hamed et al., 2011). In addition, it takes some time for the incipient particles to grow and reach detectable sizes (i.e., > 3 nm). Therefore, the reduced $N_{>3\ nm}/N_{>10\ nm}$ and $N_{3\text{-}10\ nm}$ when RH is above 80% are likely due to a combination of reduced actinic flux and recently nucleated particles having not reached detectable sizes yet in the immediate vicinity of clouds.

390
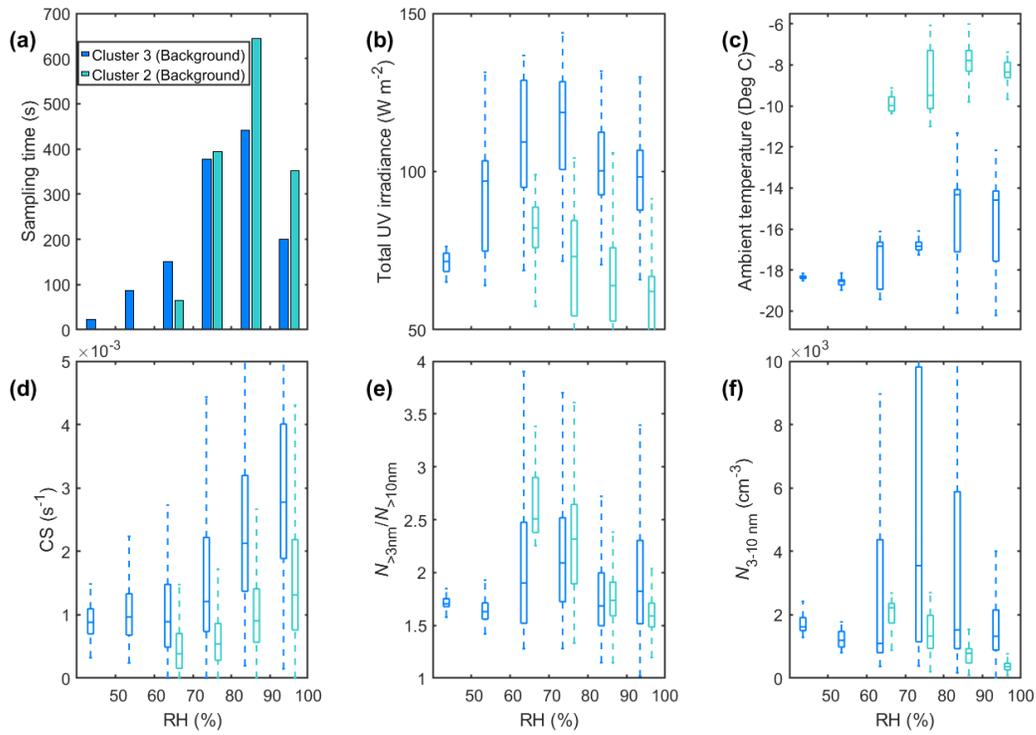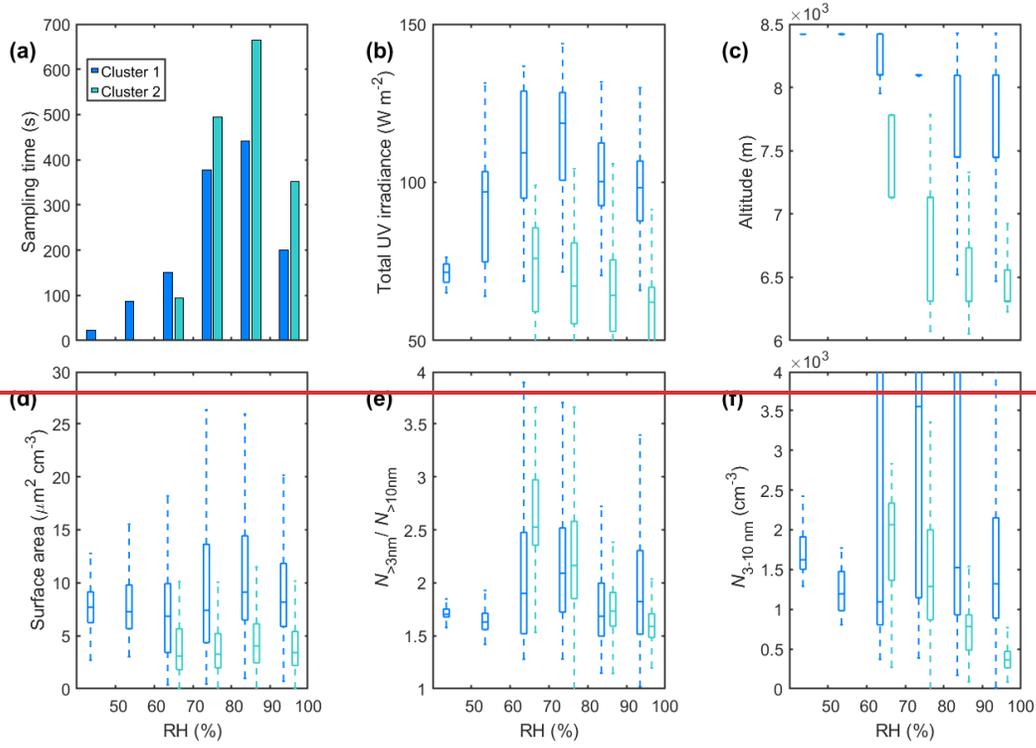
Figure 5̶4. (a) Sampling time, (b) UV irradiance, (c) altitude, (d) ~~surface area~~CS, (e) $N_{>3\ nm}$/$N_{>10\ nm}$ and (f) N_{3-10} $_{nm}$ as function of RH for two types of background NPF classified as cluster #1 and #2, respectively.

Whereas the two background NPF types share many similar features, there are also clear differences between them. The background NPF with low UV irradiance was mostly observed in the early morning, whereas in previous studies NPF was often observed later in the day when solar radiation is strong. We note that under clear sky, UV actinic flux has a weaker dependence on solar zenith angle (SZA). The UV actinic flux is estimated from the UV irradiance, SZA, and cloud condition (Details in SI). Both UV irradiance and actinic flux during the morning background NPF events are statistically lower than those during the NPF events that occurred during 10:00-14:00 in the same altitude range (Fig. S̶2S4). The median UV irradiance during morning NPF events is about 28% lower than that of the NPF events around noon, while the median UV actinic flux is about 11% lower.

One possible explanation is that these new particles were formed during the previous daytime under high UV irradiance/actinic flux, survived scavenging overnight and were detected the next morning. However, the low CS conditions are much more prevalent in the early morning than in the late afternoon (see Fig. S4 and related discussion). In addition, the frequency of NPF in the early morning is about 20 times higher than that in the afternoon suggesting that new particles observed most likely formed in the morning instead of the day before. The NPF in the early morning is likely made possible by the much lower CS despite the lower UV irradiance and actinic flux. We speculate the prevalence of low CS in the early morning is due to a combination of wet scavenging and less convection overnight. It is worth noting that nighttime NPF has been reported in conditions of low condensation sinks in the upper FT (Lee et al., 2008). However, the mechanism of nocturnal NPF is not well understood. Given the absence of nighttime measurements during the campaign, we cannot exclude the possibility that some of the new particles observed in the early morning were formed during the nighttime.
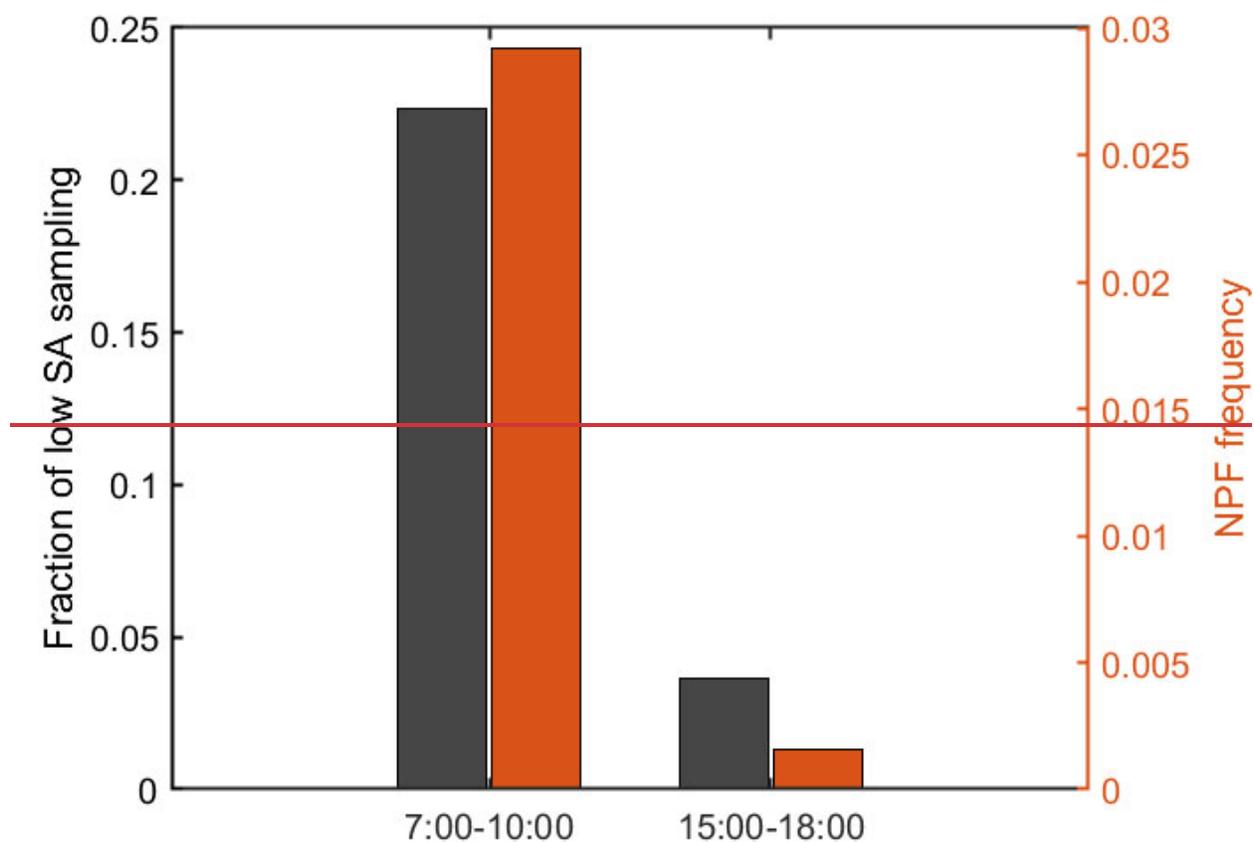
~~One possible explanation is that these new particles were formed during the previous daytime under high UV irradiance/actinic flux, survived scavenging overnight and were detected the next morning. In such a scenario, it is expected that the existing particle surface area at the time of NPF should be similar or even lower than the surface area when the new particles were observed the next morning. This is because if the surface area was reduced by wet scavenging after NPF, the newly formed particles would have been efficiently removed by coagulation with large cloud droplets, and no NPF events would be identified the next morning. Because there are no continuous measurements from late afternoon to the next morning, we statistically compare the total sampling time and the NPF frequency between early morning (7:00-10:00 local time) and late afternoon (15:00-18:00 local time) above 5 km during the whole mission, and the results are shown in Fig. 6. During CAMP²Ex, measurement periods above 5 km and after 15:00 local time are much shorter than those during 7:00-10:00. The percentage of the data with surface area below 5 μm² cm⁻³ in the early morning (i.e., 7:00-10:00) is about 22%, significantly higher than that in the late afternoon (4%, 15:00-18:00), indicating the condition of low surface area is much more prevalent during the early morning. In addition, the frequency of NPF in the early morning is about 20 times higher than that in the afternoon, suggesting that new particles observed were most likely formed in the morning, instead of the day before. Otherwise, the frequency of NPF in the afternoon would have exceeded or at least be comparable to that in the early~~

4.2 NPF Associated with Biomass Burning Smoke

Biomass burning is one of the major aerosol sources, emitting not only a large amount of primary particles but also precursors such as SO_2 (Crutzen and Andreae, 1990), DMS (Meinardi et al., 2003), and organic gases that lead to
445   secondary aerosol formation (Hennigan et al., 2012; Spracklen et al., 2011; Fiedler et al., 2011; Meinardi et al., 2003). Few direct measurements of NPF in biomass burning plumes have been reported (Shang et al., 2018; Vakkari et al., 2018; Hodshire et al., 2021). Biomass burning smoke originating from the Borneo region was sampled during the research flight on 15 September (RF9), during which high $N_{3-10\ nm}$ was observed together with a strongly enhanced CO mixing ratio (ΔCO) that is 3-5 times above typical values in background or urban-influenced air
450   masses. The NPF events in BB-influenced airmass were observed at 6.7 km. A HYSPLIT-based five-day backward trajectory analysis was simulated using similar methods to a previous measurement report (Hilario et al., 2021) for air masses arriving at different sampling altitudes of RF9 on 15 September 2019. Within the boundary layer, the prevailing wind was from the southwest, and airmasses originated from Borneo regions, where strong biomass burning activities were reported. In contrast, air masses arriving at 6.7 km came from the west Pacific with no direct
455   influence by biomass burning (Fig. ~~S3~~S6). The BB-influenced air mass observed in the FT during RF9 is therefore due to the vertical lifting and detrainment of the biomass burning plume by convective clouds, instead of direct long-range transport inside the FT from Borneo. The biomass burning plume had travelled inside the boundary layer across the Sulu Sea from the Borneo (Fig. ~~S3~~S6), consistent with previous findings that transport of smoke to the region mostly occurred within boundary layer due to strong wind shear during the southwest Monsoon season
460   (Hilario et al., 2020; Xian et al., 2013).

To investigate the potential impact of biomass burning emissions on NPF, we compare NPF observed during RF9 to background NPF from other flights within the same altitude range. Because no measurements of non-methane hydrocarbons are available during CAMP²Ex, we use CO as a surrogate for VOCs emitted from biomass burning. As UV irradiance plays an important role in NPF, the key variables including $N_{>3\ nm}/N_{>10\ nm}$ and $N_{3-10\ nm}$ during both
465   BB-influenced and background NPF events are compared for the same UV irradiance levels (Fig. ~~7~~5) such that the role of precursors can be clearly differentiated from other factors~~.~~
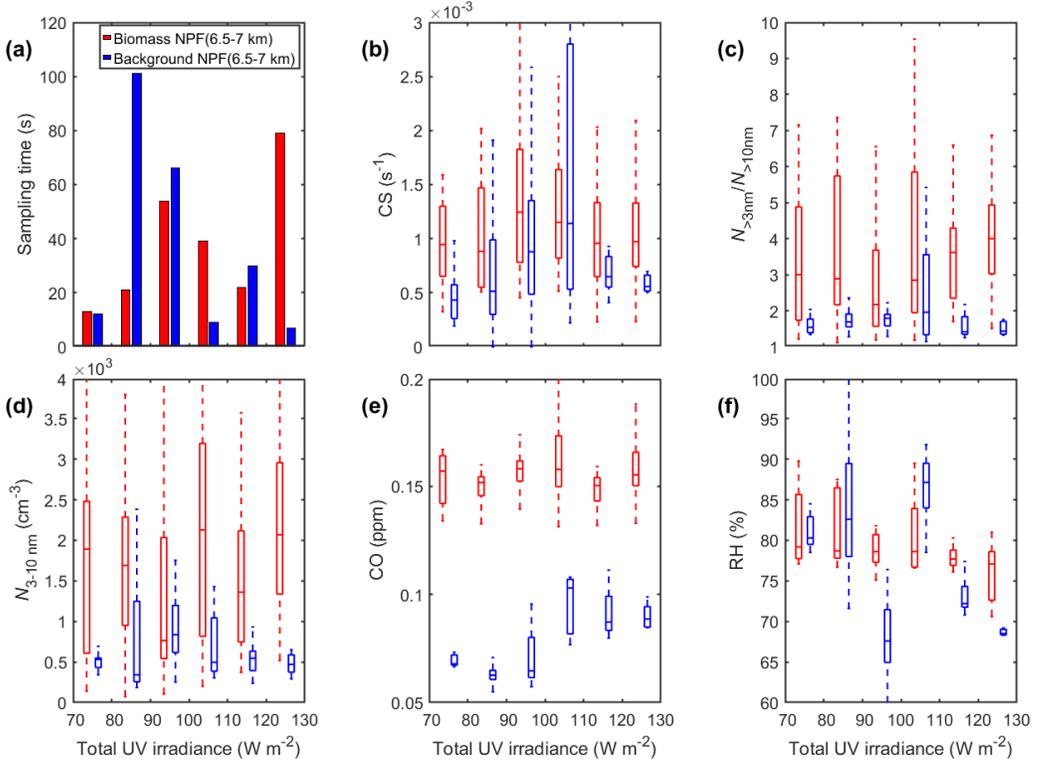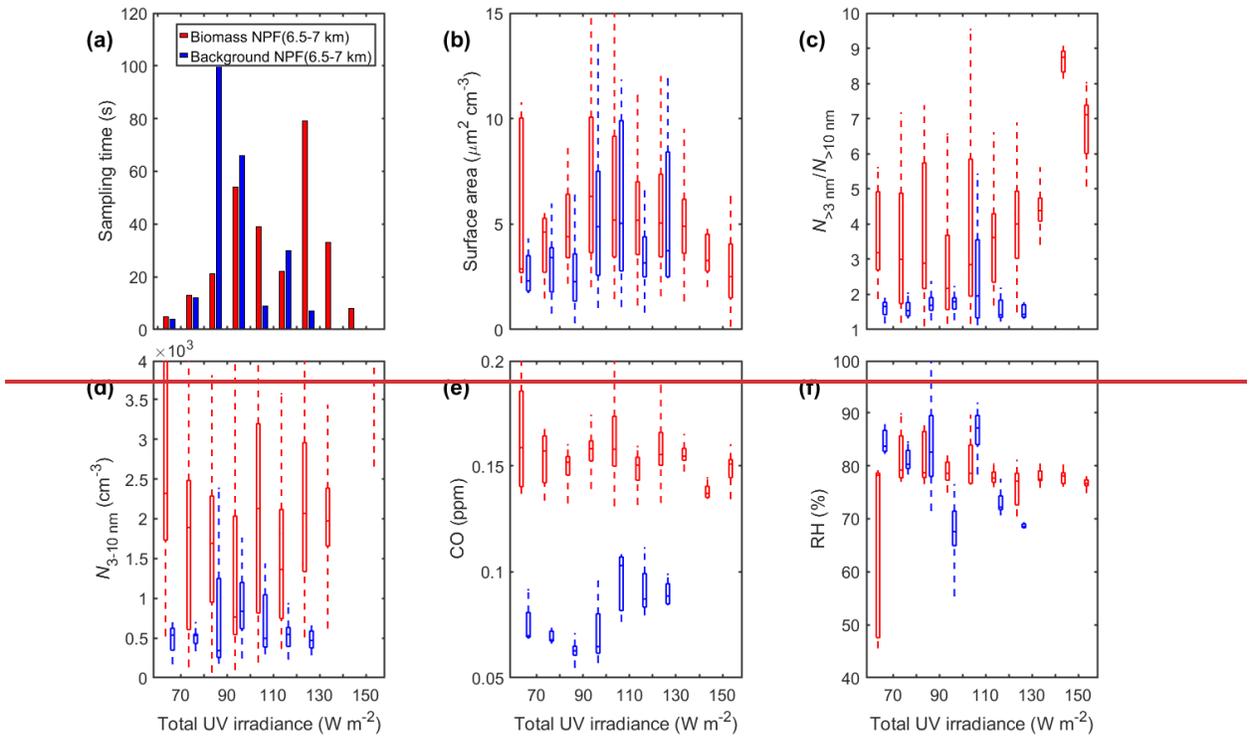
Figure ~~7~~5. Comparison between NPF influenced by biomass burning smoke and NPF in background. (a)
Sampling time, (b) ~~surface area~~CS, (c) $N_{>3\ nm}/N_{>10\ nm}$, (d) $N_{3-10\ nm}$, (e) CO and (f) RH are plotted as a function
of UV irradiance.

We focus on the comparison for UV irradiance ranging from 70-130 W m^{-2} based on background NPF such that the
amount of data ~~sizes~~ for both NPF types are comparable. There exists a substantial fraction of BB-influenced NPF
with UV irradiance higher than 130 W m^{-2}, whereas few non-BB NPF events at the same altitude range had UV
irradiance above 130 W m^{-2}. ~~For~~ At the same UV irradiance level, BB-influenced NPF occurred with similar or
slightly higher ~~surface area~~CS compared to the background NPF (Fig. ~~5~~7b) but with much stronger intensity (i.e.,
$N_{>3\ nm}/N_{>10\ nm}$ and $N_{3-10\ nm}$, Fig. ~~7c~~5c, ~~7d~~5d). ~~The stronger NPF in the BB-influenced airmass at the same UV~~
~~irradiance level and similar or slightly higher surface area~~This indicates that precursors emitted by biomass burning
enhances NPF, as indicated by elevated CO mixing ratio (Fig. ~~7e~~5e). The ~~similar or only slightly higher surface~~
~~area~~CS of BB-influenced NPF events suggests that the existing particles were efficiently removed through wet
scavenging as the biomass burning plume was lifted into the FT by the convective clouds. Despite a high
concentration of precursors, the efficient removal of existing particles appears to be a necessary condition for NPF
to occur in the aged BB-influenced air masses. There are two leveled flight segments at the same altitude of 6.7 km
during RF9 (times series shown in Fig. S7). NPF was observed during one segment with much reduced ~~surface~~
~~area~~CS and non-volatile particle concentration (Fig. S7, 12:45-12:55). For the other segment (Fig. S7, 11:15-11:25),
the concentrations of non-volatile particles and larger particles (> 100 nm) were three times as high as ~~when~~ those of
the NPF ~~was absent~~events (Fig. S4). It remains unclear which nucleation pathway dominates particle formation
observed in BB-influenced air mass, since organic vapors, ammonia (Hegg et al., 1988) and sulfuric acid can
directly or indirectly originate from biomass burning plumes and contribute to formation of secondary aerosols
(Ahern et al., 2019). In terms of potential organic precursors, oxygenated aromatics together with heterocyclic
compounds were reported to account for almost 80% of total mass of secondary aerosols (Akherati et al., 2020), and
mixtures of sulfuric acid, ammonia and organic vapors have been shown leading to strong NPF (Lehtipalo et al.,
2018). Other laboratory studies reported that oxidized aromatic VOCs such as benzenediols, phenols and
benzaldehyde were dominant potential precursors (Gilman et al., 2015; Yee et al., 2013). More measurements are
required to investigate nucleation mechanisms in air masses influenced by biomass burning plumes and the potential
impact of aging and scavenging during long-range transport.

4.3 NPF Influenced by Urban Emissions

Besides background and BB-influenced NPF, NPF events were also observed in many air masses influenced by
urban emissions. These urban-influenced NPF events exhibit quite different conditions, (e.g., RH, ~~surface area~~CS~~),~~
~~and)~~ and are classified into different k-means clusters. Therefore, the discussion of NPF in air masses influenced by
urban emissions (~~urban~~ urban-influenced NPF, hereafter) will follow the classification by k-means clustering (see
Fig. ~~4~~3). A large fraction of cluster #~~3~~ 1 is classified as urban-influenced, which is mostly from RF7 and RF8 at an
altitude of 5.5-6.5 km, while a small fraction of cluster #~~1~~ 3 and ~~entire~~ the majority of cluster #4 represent urban
influenced NPF at altitudes above 7 km. The remain~~der~~sing are distributed throughout cluster #5-6 and exhibit

505   contrasting features, i.e., occurring with elevated ~~surface area~~CS ~~compared to the non-NPF periods at comparable altitudes~~ (Fig. ~~4c~~3c).

4.3.1 NPF over Coastal Regions and Land at Altitudes of 5.5-6.5 km

~~Urban~~ Urban-influenced NPF classified as cluster #~~3~~1 share~~s~~ some similar features with the NPF observed in BB-influenced air masses. The locations of these ~~urban~~ urban-influenced NPF events are shown in Fig. ~~S5~~S8.

510   Measurements on 13 September 2019 show elevated $N_{>3 \text{ nm}}/N_{>10 \text{ nm}}$ and $N_{3\text{-}10 \text{ nm}}$ during the level flight near Manila. In addition, on 8 September 2019, extremely high $N_{>3 \text{ nm}}/N_{>10 \text{ nm}}$ values up to 40 and $N_{3\text{-}10 \text{ nm}}$ above 4000 cm^{-3} were observed at altitudes of ~6.3 km over the West Pacific about 50 km away from the coastline. These events together represent over ~~80~~70% of ~~data classified as~~ cluster #~~3~~1, and the general features include low ~~surface area~~CS, high UV irradiance and high RH, similar to BB-influenced NPF events.
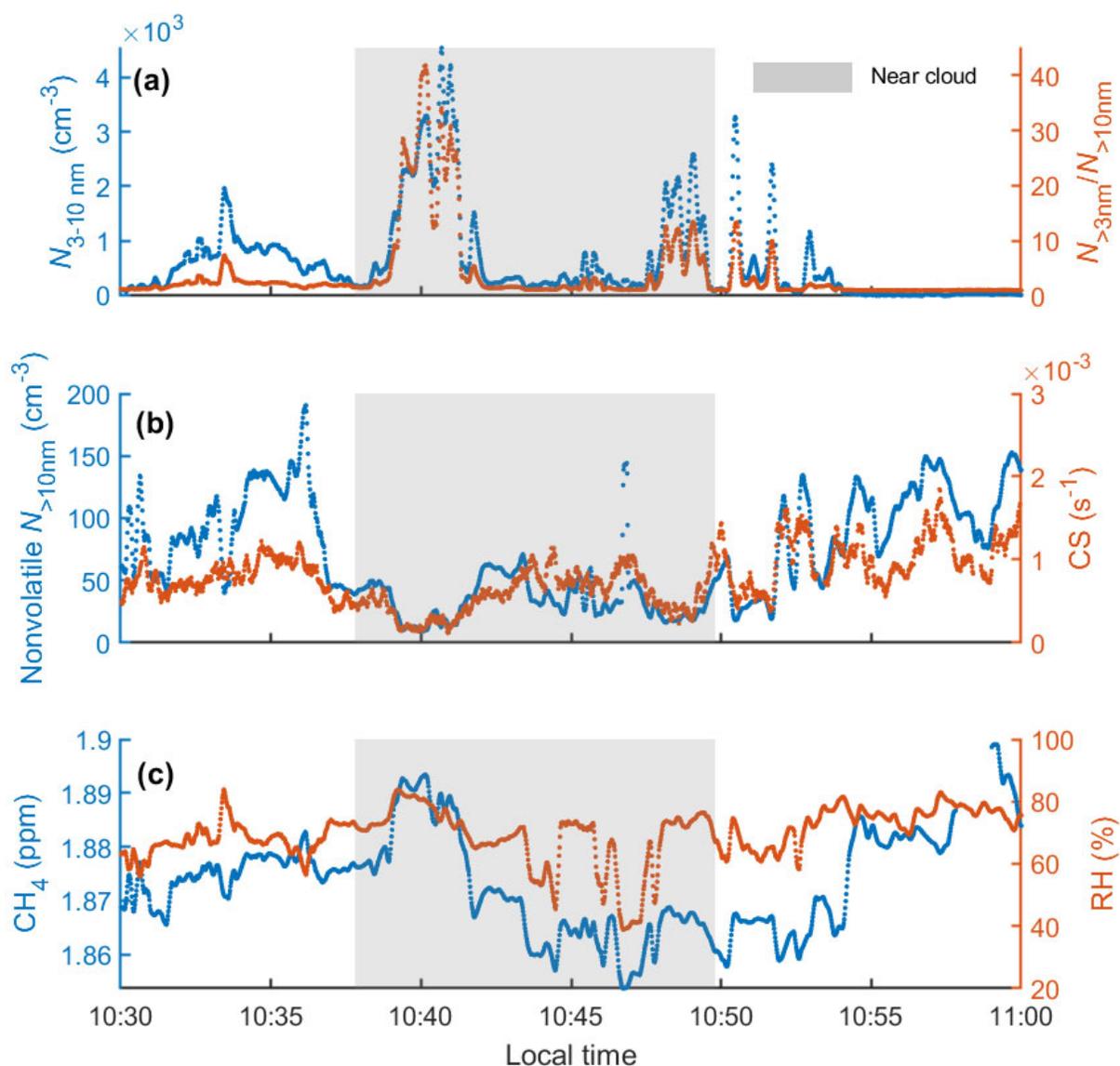
515

Figure 8̶6. Time series plot for a segment with NPF observed in an ~~urban emission~~urban-­influenced air mass near cumulus clouds during RF7 (10:37-10:50, 8 September 2019), including (a) $N_{3\text{-}10\ nm}$ and $N_{>3\ nm}/N_{>10\ nm}$, (b) number concentration of non-volatile particles lager than 10 nm and ~~surface area~~CS, and (c) CH_4 mixing ratio and RH.

520   Figure ~~8~~6 shows the key variables during a representative urban-influenced NPF event, which was observed over the ocean east of Luzon during RF7. The time series shows drastically increased $N_{>3\ nm}/N_{>10\ nm}$ and elevated CH_4 concentration around 10:40, which were observed near convective clouds based on video from the forward-looking camera. Starting from ~10:35, both the ~~surface area~~CS and concentration of non-volatile particles (nonvolatile $N_{>10\ nm}$) decrease, while RH and CH_4 concentration become elevated, indicating the uplift of humid and ~~urban~~urban-

525 influenced air from lower altitude. The concurrence of drastically increased $N_{>3\,nm}/N_{>10\,nm}$ and elevated CH_4 suggests trace gases emitted in urban areas contribute to the production of nucleating species and NPF. Here CH_4 is used as a surrogate for emitted precursors in urban plumes, which typically include SO_2, gaseous sulfuric acid and organic species (Zhang et al., 2012). A similar positive correlation between $N_{>3\,nm}/N_{>10\,nm}$ and CH_4 concentration is also found during the leveled box flight segment of RF8, which took place close to Manila (not shown). Compared to

530 most other NPF events, these events were observed closer to urban areas over the land and are therefore more likely influenced by fresh urban emissions. The contribution of urban emitted trace gases to the NPF ~~This~~ is also supported by statistical comparison~~sing~~ ~~the~~of CH_4 concentration, UV irradiance, and RH between such NPF events and non-NPF periods at the same altitude (5.5-6.5 km) and time of day ~~range~~ as a function of CS (~~as shown in~~ Fig. S9 and related discussion). When CS is below 0.0015 s^{-1}, urban-influenced NPF has a similar level of UV irradiance but

535 higher CH_4 concentration and RH compared to the non-NPF periods, suggesting that precursors emitted from urban areas likely contribute to the formation of nucleation species and NPF ~~(Supplementary Information)~~.

~~Given the dependence of NPF on multiple parameters (e.g., surface area, UV irradiance, and precursor concentrations), the potential impact of urban emissions on NPF is examined statistically. One approach is to statistically compare $N_{>3\,nm}/N_{>10\,nm}$ and $N_{3-10\,nm}$ between urban-influenced NPF (i.e., classified in cluster #3) and~~

540 ~~background NPF events under same conditions (i.e., altitude, surface area, RH, and UV irradiance). However, such comparison is not possible as most background NPF events observed at similar altitudes had substantially lower UV irradiance (below 100 W m^{-2}, cluster #2). As a result, the impact of urban emission on NPF was examined by statistically comparing urban-influenced NPF and non-NPF events at the similar altitude range and time of the day (i.e., solar radiation) as a function of surface area. Figure 9 shows that urban-influenced NPF occurred mostly with~~

545 ~~surface area less than ~ 6 µm² cm⁻³, substantially lower than during most of the non-NPF periods. For surface areas below 6 µm² cm⁻³, the UV irradiance and RH are statistically similar between urban-influenced NPF events and non-NPF periods, whereas urban-influenced NPF events show elevated CH_4 concentration. This suggests that precursors emitted from urban areas likely contribute to the formation of nucleating species and NPF.~~

4.3.2 NPF Influenced by Aged Urban Plume

Part of cluster ~~#1~~ #3 and cluster #4 represent urban-influenced NPF observed at higher altitudes (~7-8.1 km) than urban-influenced NPF observed ~~between 5.5 and~~(5.5-6.5 km). In addition to the difference in altitude ~~range~~, these NPF events were observed over the ocean and exhibit relatively lower RH (below 50%) and/or higher ~~surface area~~CS (the median CS of cluster #3 is above ~~10 μm²~~0.001 ~~scm~~ ~~cm⁻¹~~). Figure ~~10~~ 7 shows representative examples of such NPF events, which were observed during RF10 over the west Pacific and 600 km away from the coast. During the NPF events, $N_{>3\,nm}/N_{>10\,nm}$ and $N_{3\text{-}10\,nm}$ reached 3 and 2000 cm⁻³, respectively. The elevated $N_{>3\,nm}/N_{>10\,nm}$ and $N_{3\text{-}10\,nm}$ coincide with elevated RH and reduced ~~surface area~~CS ~~(Fig. 10a-c)~~, and both $N_{>3\,nm}/N_{>10\,nm}$ and RH are anti-

correlated with CH$_4$ concentration during the period (~~11:25-11:32~~ ~~Fig. 10a, 10c~~), indicating particle formation in cloud outflow regions with reduced CH$_4$ concentration. Back-trajectories and elevated CH$_4$ level (i.e., around 1.9 ppm) suggest the air mass at the sampling altitude was influenced by aged urban plumes transported from East Asia. The anti-correlations between RH and CH$_4$ indicate that humid background (i.e., low CH$_4$ concentration) air was lifted by convective clouds and mixed into the aged urban plume. We expect the reactive precursors in the aged urban plume were mostly consumed during the long-range transport, while CH$_4$ concentration and ~~existing particle surface area~~CS remain relatively high due to longer lifetimes in the FT. As a result, NPF only occurs when the aged plume is mixed with sufficient air detrained from convective clouds, which is expected to have reduced ~~surface area~~CS and elevated concentration of reactive gases such as DMS. Therefore, the aged urban plume tends to suppress NPF instead of promoting it, as in air masses influenced by fresh urban emissions shown in Sect. 4.3.1.
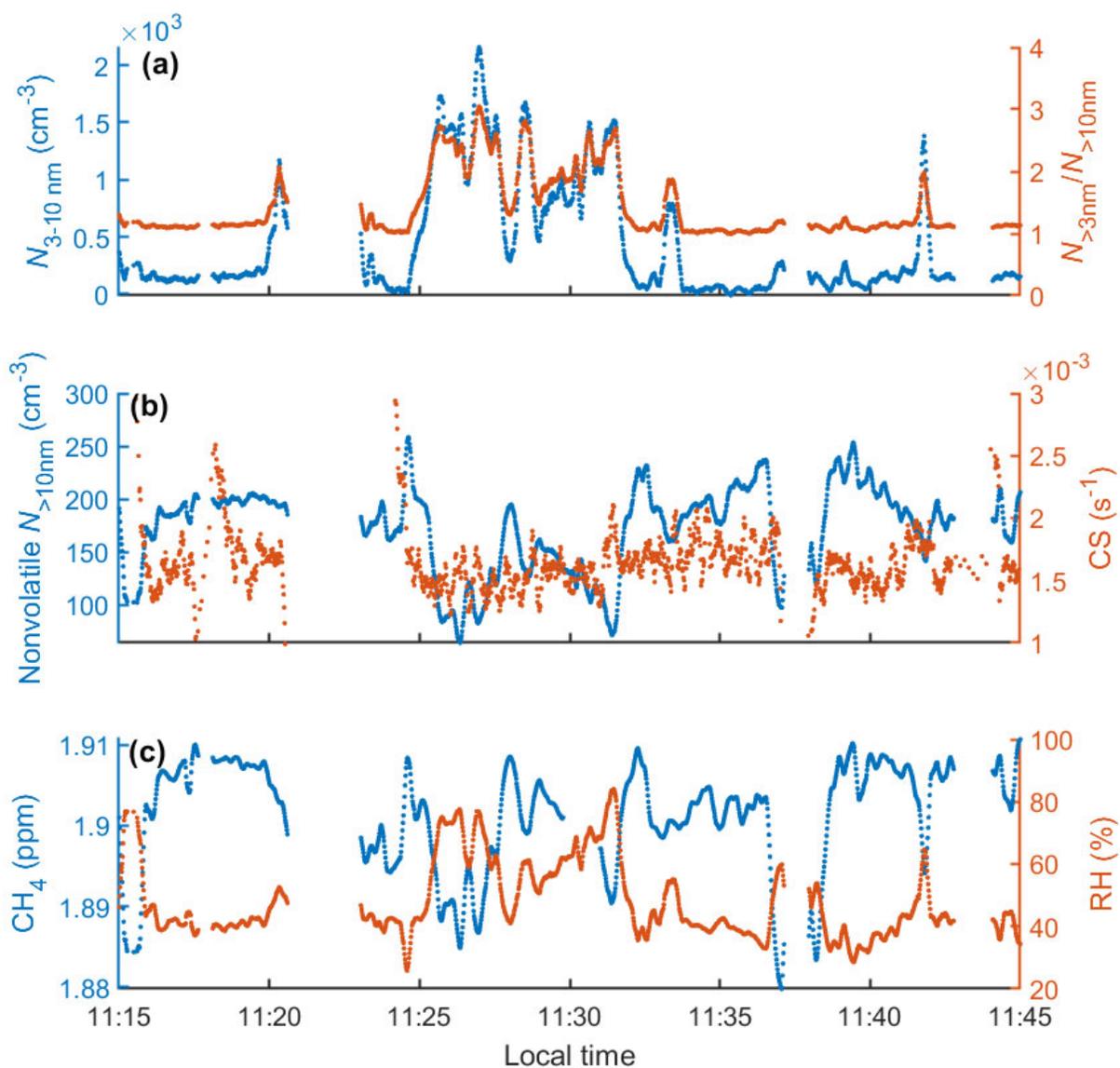
Figure ~~10~~7. Time series plot of a level flight segment from RF10 (16 September 2019) where NPF was observed, including (a) $N_{3\text{-}10\,nm}$ and $N_{>3\,nm}/N_{>10\,nm}$, (b) number concentration of non-volatile particles lager than 10 nm and CS, and (c) CH_4 mixing ratio and RH.

4.3.3 Urban Influenced NPF with High ~~Surface Area~~CS

Unlike most NPF events during CAMP²Ex, a small fraction of urban influenced NPF events occurred with high ~~surface area~~CS. These events were grouped into different clusters (i.e., clusters #5 and #6) by the k-means clustering method. Figure ~~11~~S10 shows increasing $N_{3\text{-}10\,nm}$ with concentration of accumulation mode particles (i.e., $N_{>100\,nm}$) during some examples of such NPF events. These examples were observed at 4.8 km (~0 °C) over Metro Manila during RF18, which was designed to sample urban plumes from Metro Manila. As new particles are typically formed ~~when the concentration of existing large particles is low~~under low CS conditions, a negative correlation between $N_{3\text{-}10\,nm}$ and $N_{>100\,nm}$ is expected. The positive correlation, together with the sampling location, suggests that both $N_{3\text{-}10\,nm}$ and the accumulation mode particles might originate from primary emissions in Metro Manila. Previous studies show that aerosol particles with diameters of a few nanometers can form as the fresh exhaust from diesel/gasoline engines rapidly cools. While these nanoparticles are formed through nucleation, they are often considered "primary" as the nucleation process occurs very close to the sources (Uhrner et al., 2011; Wehner et al., 2009). If the elevated $N_{3\text{-}10\,nm}$ was due to primary emissions in metro Manila, we would expect even higher $N_{3\text{-}10\,nm}$ at lower altitudes. However, no NPF events were identified when P-3B sampled in the metro Manila regions below 4.8 km. In addition, albeit from a different flight, the vertical profiles of aerosol and trace gases during a descending leg over Lingayen Gulf (RF8, Fig. ~~12~~S11) show that the small particles with diameters between 3 and 10 nm are secondary despite a positive correlation between $N_{3\text{-}10\,nm}$ and $N_{>100\,nm}$. The vertical profiles show several detrainment layers with elevated $N_{3\text{-}10\,nm}$ from 2.5 km up to 4.5 km, whereas the small particles were mostly absent below 2.5 km. ~~It is worth noting that only the segment of 4-4.5 km was identified as an NPF event due to its sufficiently long duration (i.e., more than 30 seconds). In individual detrainment layers, surface area, CO, and CH₄ are locally enhanced, and $N_{3\text{-}10\,nm}$ can be positively correlated with $N_{>100\,nm}$ as observed in the layer around 3.4 km.~~ The comparisons among the different layers show that $N_{3\text{-}10\,nm}$ increases while $N_{>100\,nm}$, ~~surface area~~CS, and CO decrease with altitude, indicating the observed small particles were formed in the detrainment layers instead of originating from the primary emissions near the surface. The mechanism for this type of NPF is likely similar to those observed in polluted urban boundary layers (Alam et al., 2003; Zhu et al., 2014; Yao et al., 2018), where high concentrations of precursors make nucleation and particle formation possible despite the high CS conditions. ~~The absence of NPF below 2 km suggest the scavenging of existing particles, while not as pronounced as during the NPF events observed at higher altitudes (e.g., >6 km), still plays an important role in NPF in these detrainment layers below 5 km.~~ The absence of NPF below 2 km may result from a combination of higher condensation sink and warmer temperature compared to those in the detrainment layers at higher altitudes. Stolzenburg et al. (2018) show that temperature impacts the growth by organics via competing processes. While a higher temperature leads to faster reaction rate and high concentration of highly oxidized molecules, it also strongly increases the volatility of organic species, therefore slowing down or even inhibiting the condensation of organic vapors onto the newly formed clusters.
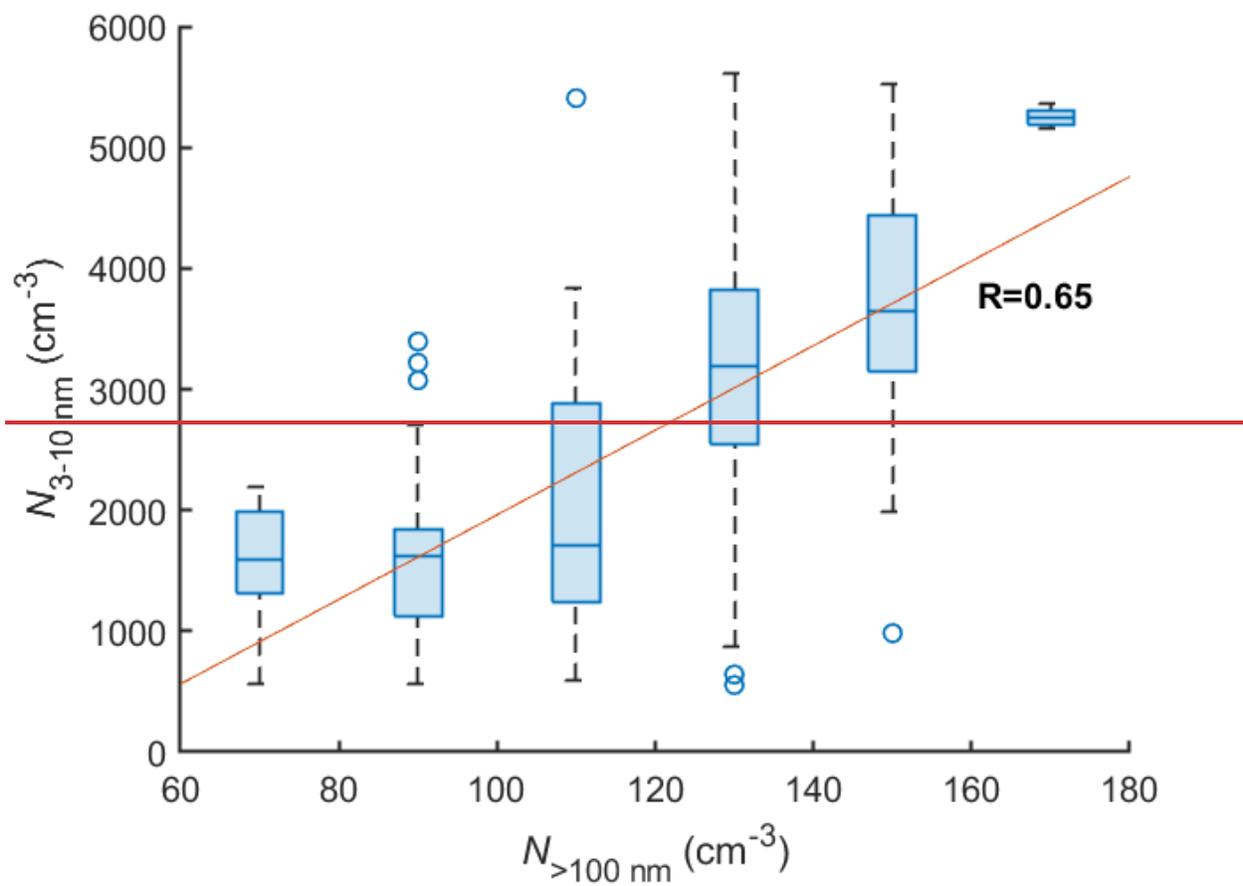
610

Figure 11. Box whisker plots of $N_{3-10\,nm}$ for different $N_{>100\,nm}$ bins during the NPF event observed during RF18 (3 October 2019) over Metro Manila. The $N_{>100\,nm}$ bins have a width of 20 cm⁻³ (i.e., 60-80 cm⁻³, 80-100 cm⁻³..., 160-1180 cm⁻³). Orange line represents a linear fit of all 170 individual data points (R=0.65).
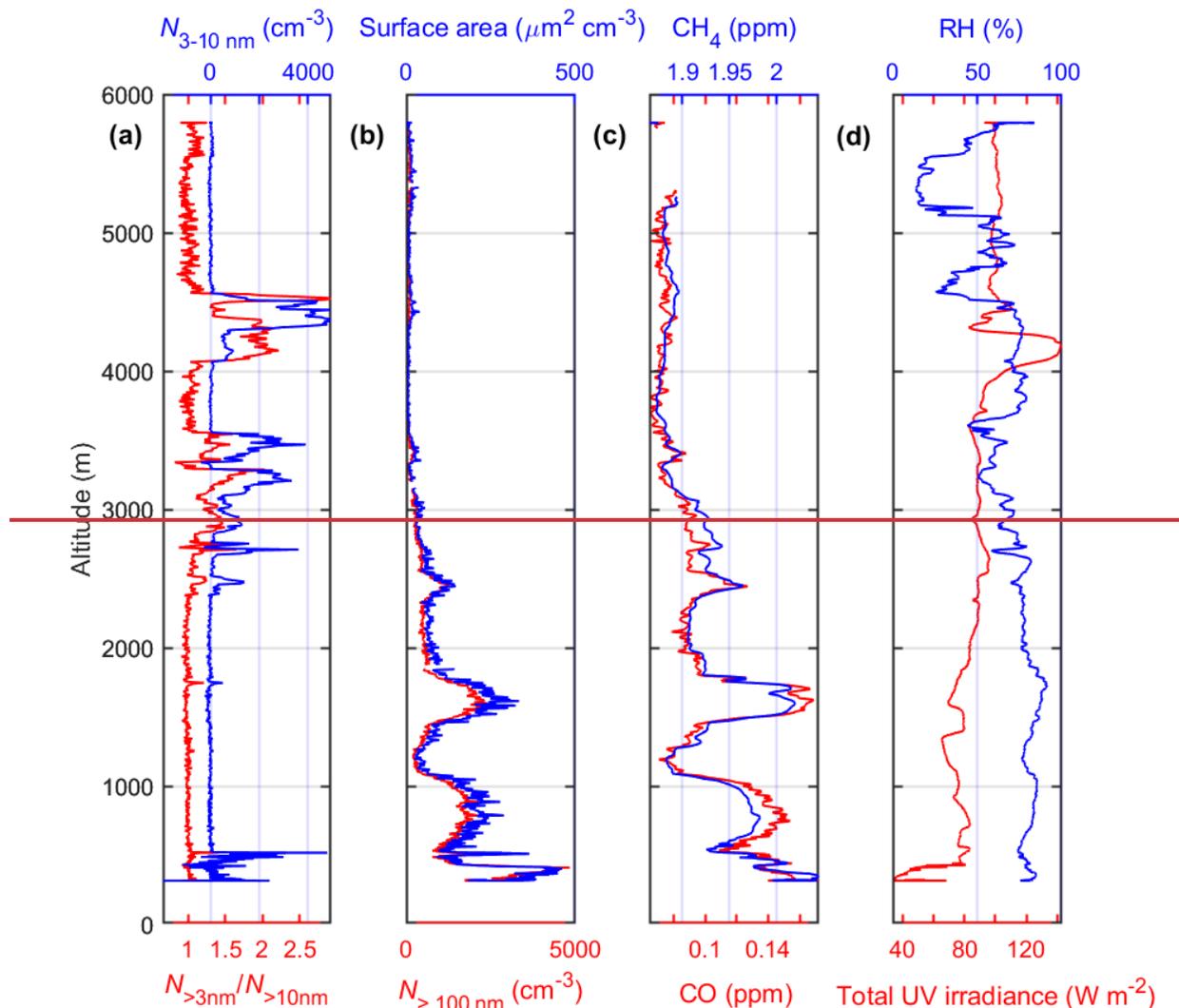
5 Summary

In this study, we examine NPF events in the tropical FT in the altitude range of 3-8.5 km using airborne measurements collected during CAMP²Ex campaign. NPF events were classified based on air mass types, including background, biomass burning influenced, and ~~urban~~ urban-influenced. The features of key variables, including RH, ~~surface area~~CS, UV irradiance as well as concentrations of trace gases are presented for different NPF types and over different altitude ranges. The impact of air mass types on the NPF is investigated. We summarize key conclusions as follows:

1) Most of the NPF events were observed above 6 km in air that was processed by convective clouds and with low ~~existing aerosol surface area~~CS. No newly formed particles were observed below 3 km, possibly due to

high temperature and high ~~condensation sink~~CS. Below 6 km, NPF was rare and mostly observed in urban influenced air, likely due to abundant precursors emitted from urban areas. Above 6 km, NPF frequency increases with altitude, reaching about 49% at 8 km, and NPF frequency in background air was usually higher than in urban influenced air masses. There is a drastic decrease in NPF frequency from the southwest monsoon to the monsoon transition, coinciding with a statistical decrease in RH and increase in ~~surface area~~CS in the FT. The decrease of NPF frequency during the monsoon transition phase is attributed to the decrease of convective activity and thus less efficient removal of existing aerosol particles associated with altered meteorological conditions.

2) NPF in background air was observed under two different types of conditions. One type was observed around noon time in the vicinity of clouds, with high RH (above 70%), ~~reduced surface area~~low CS, and strong UV irradiance. The second type was observed in the early morning with some of lowest ~~surface area~~CS observed during CAMP^{2}Ex. The very low ~~surface area~~CS is attributed to a combination of wet-scavenging and less convection (i.e., reduced vertical transport of aerosol particles from near surface to the FT) over night. NPF in the morning is likely made possible by the much lower ~~surface area~~CS ~~(i.e., condensation sink for the nucleating species)~~, despite the lower UV irradiance and calculated actinic flux compared to noon time periods at the same altitudes.

3) The impact from biomass burning and urban emissions on NPF is investigated. During CAMP^{2}Ex, the impact of urban emission on NPF shows a clear altitude dependence. Between 5.5 and 7 km, urban influenced and biomass burning influenced NPF were observed with ~~reduced surface area~~low CS and enhanced UV irradiance near clouds. The elevated concentrations of precursors from either urban emission or biomass burning enhances the formation of nucleating species and NPF. Urban-influenced NPF was usually observed close to the land where the influence of fresh urban emissions is expected.

4) Above 7 km, ~~urban~~urban-influenced NPF was observed when the background humid air was lifted by convective clouds and mixed into the aged urban plume. The reactive precursors in the aged urban plume were mostly consumed during the long-range transport from East Asia, while ~~existing particle surface area~~CS remained relatively high due to longer aerosol lifetime in the FT. As a result, the aged urban plume tends to inhibit NPF instead of promoting it as is the case with air masses influenced by fresh urban emissions at lower altitudes.

5) A small number of urban-influenced NPF events were observed with high ~~existing aerosol surface area~~CS. The vertical profile of particle number concentrations indicates that the small particles were formed in the detrainment layers instead of originating from the primary emissions near the surface. High concentrations of precursors from urban emissions likely made NPF possible despite relatively high ~~existing surface area~~CS.

The results from this study highlight the role of convective clouds that efficiently scavenge existing aerosol particles, inject reactive precursors into the FT, and enhance UV irradiance, all of which facilitate nucleation and particle formation. The results also show competing influences of different variables and complex interactions between anthropogenic emissions, transport, convective clouds, and meteorology, which lead to NPF under a variety

of conditions and altitudes. Due to the lack of measurements of precursors, the nucleation pathways of NPF in different air mass types are not well understood and should be examined in future studies. The impact of urban and

665 biomass burning emissions on NPF, and subsequent formation of cloud condensation nuclei will also need to be examined in the future by combining field observations and model simulations.

Data Availability. CAMP^{2}Ex observational datasets are available at https://asdc.larc.nasa.gov/project/CAMP2Ex. HYSPLIT data are accessible through the NOAA READY website (http://www.ready.noaa.gov). The code used to generate the figures is available upon request.

670 *Author Contributions.* JW and QX designed the study. JZ, YW, LZ, EC, EW, CR, JD, GD, KS, SW, SS, and PL carried out the measurements and data reduction. QX and JW led the data analysis and the preparation of manuscript, with contributions from all authors. We thank Michael Jones and Adam Bell for their comments on the manuscript.

Competing interests. One of the co-authors is a member of the editorial board of *Atmospheric Chemistry and*
675 *Physics*. The peer-review process was guided by an independent editor, and the authors have also no other competing interests to declare.

Acknowledgement. We acknowledge the funding support from National Aeronautics and Space Administration (grant no. 80NSSC19K0618).

References

680 Ahern, A. T., Robinson, E. S., Tkacik, D. S., Saleh, R., Hatch, L. E., Barsanti, K. C., Stockwell, C. E., Yokelson, R. J., Presto, A. A., Robinson, A. L., Sullivan, R. C., and Donahue, N. M.: Production of Secondary Organic Aerosol During Aging of Biomass Burning Smoke From Fresh Fuels and Its Relationship to VOC Precursors, Journal of Geophysical Research: Atmospheres, 124, 3583-3606, https://doi.org/10.1029/2018JD029068, 2019.

Akherati, A., He, Y., Coggon, M. M., Koss, A. R., Hodshire, A. L., Sekimoto, K., Warneke, C., de Gouw, J., Yee, 685 L., Seinfeld, J. H., Onasch, T. B., Herndon, S. C., Knighton, W. B., Cappa, C. D., Kleeman, M. J., Lim, C. Y., Kroll, J. H., Pierce, J. R., and Jathar, S. H.: Oxygenated Aromatic Compounds are Important Precursors of Secondary Organic Aerosol in Biomass-Burning Emissions, Environmental Science & Technology, 54, 8568-8579, 10.1021/acs.est.0c01345, 2020.

Alam, A., Shi, J. P., and Harrison, R. M.: Observations of new particle formation in urban air, Journal of 690 Geophysical Research: Atmospheres, 108, https://doi.org/10.1029/2001JD001417, 2003.

Andreae, M. O., Afchine, A., Albrecht, R., Holanda, B. A., Artaxo, P., Barbosa, H. M. J., Borrmann, S., Cecchini, M. A., Costa, A., Dollner, M., Fütterer, D., Järvinen, E., Jurkat, T., Klimach, T., Konemann, T., Knote, C., Krämer, M., Krisna, T., Machado, L. A. T., Mertes, S., Minikin, A., Pöhlker, C., Pöhlker, M. L., Pöschl, U., Rosenfeld, D., Sauer, D., Schlager, H., Schnaiter, M., Schneider, J., Schulz, C., Spanu, A., Sperling, V. B., Voigt, C., Walser, A., 695 Wang, J., Weinzierl, B., Wendisch, M., and Zireis, H.: Aerosol characteristics and particle production in the upper troposphere over the Amazon Basin, Atmos. Chem. Phys., 18, 921-961, 10.5194/acp-18-921-2018, 2018.

Arthur, D. and Vassilvitskii, S.: k-means++: the advantages of careful seeding, Proceedings of the eighteenth annual ACM-SIAM symposium on Discrete algorithms, New Orleans, Louisiana2007.

Baier, B. C., Sweeney, C., Choi, Y., Davis, K. J., DiGangi, J. P., Feng, S., Fried, A., Halliday, H., Higgs, J., and 700 Lauvaux, T.: Multispecies assessment of factors influencing regional CO2 and CH4 enhancements during the winter 2017 ACT-America campaign, Journal of Geophysical Research: Atmospheres, 125, e2019JD031339, 2020.

Chae, J. H., Wu, D. L., Read, W. G., and Sherwood, S. C.: The role of tropical deep convective clouds on temperature, water vapor, and dehydration in the tropical tropopause layer (TTL), Atmos. Chem. Phys., 11, 3811-3821, 10.5194/acp-11-3811-2011, 2011.

705 Chen, H., Schmidt, S., King, M. D., Wind, G., Bucholtz, A., Reid, E. A., Segal-Rozenhaimer, M., Smith, W. L., Taylor, P. C., Kato, S., and Pilewskie, P.: The effect of low-level thin arctic clouds on shortwave irradiance: evaluation of estimates from spaceborne passive imagery with aircraft observations, Atmos. Meas. Tech., 14, 2673-2697, 10.5194/amt-14-2673-2021, 2021.

Clarke, A. D., Varner, J. L., Eisele, F., Mauldin, R. L., Tanner, D., and Litchy, M.: Particle production in the remote 710 marine atmosphere: Cloud outflow and subsidence during ACE 1, Journal of Geophysical Research: Atmospheres, 103, 16397-16409, https://doi.org/10.1029/97JD02987, 1998.

Clarke, A. D., Eisele, F., Kapustin, V., Moore, K., Tanner, D., Mauldin, R., Litchy, M., Lienert, B., Carroll, M. A., and Albercook, G.: Nucleation in the equatorial free troposphere: Favorable environments during PEM-Tropics, Journal of Geophysical Research, 104, 5735-5744, 10.1029/98JD02303, 1999.

715 Corral, A. F., Choi, Y., Crosbie, E., Dadashazar, H., DiGangi, J. P., Diskin, G. S., Fenn, M., Harper, D. B., Kirschler, S., Liu, H., Moore, R. H., Nowak, J. B., Scarino, A. J., Seaman, S., Shingler, T., Shook, M. A., Thornhill, K. L., Voigt, C., Zhang, B., Ziemba, L. D., and Sorooshian, A.: Cold Air Outbreaks Promote New Particle Formation Off the U.S. East Coast, Geophysical Research Letters, 49, e2021GL096073, https://doi.org/10.1029/2021GL096073, 2022.

720 Crumeyrolle, S., Manninen, H. E., Sellegri, K., Roberts, G., Gomes, L., Kulmala, M., Weigel, R., Laj, P., and Schwarzenboeck, A.: New particle formation events measured on board the ATR-42 aircraft during the EUCAARI campaign, Atmos. Chem. Phys., 10, 6721-6735, 10.5194/acp-10-6721-2010, 2010.

Crutzen, P. J. and Andreae, M. O.: Biomass Burning in the Tropics: Impact on Atmospheric Chemistry and Biogeochemical Cycles, Science, 250, 1669-1678, doi:10.1126/science.250.4988.1669, 1990.

725 Dada, L., Paasonen, P., Nieminen, T., Buenrostro Mazon, S., Kontkanen, J., Peräkylä, O., Lehtipalo, K., Hussein, T., Petäjä, T., Kerminen, V. M., Bäck, J., and Kulmala, M.: Long-term analysis of clear-sky new particle formation events and nonevents in Hyytiälä, Atmos. Chem. Phys., 17, 6227-6241, 10.5194/acp-17-6227-2017, 2017.

Dadashazar, H., Braun, R. A., Crosbie, E., Chuang, P. Y., Woods, R. K., Jonsson, H. H., and Sorooshian, A.: Aerosol characteristics in the entrainment interface layer in relation to the marine boundary layer and free
730 troposphere, Atmos. Chem. Phys., 18, 1495-1506, 10.5194/acp-18-1495-2018, 2018.

Dal Maso, M., Kulmala, M., Lehtinen, K. E. J., Mäkelä, J. M., Aalto, P., and O'Dowd, C. D.: Condensation and coagulation sinks and formation of nucleation mode particles in coastal and boreal forest boundary layers, Journal of Geophysical Research: Atmospheres, 107, PAR 2-1-PAR 2-10, https://doi.org/10.1029/2001JD001053, 2002.

DiGangi, J. P., Choi, Y., Nowak, J. B., Halliday, H. S., Diskin, G. S., Feng, S., Barkley, Z. R., Lauvaux, T., Pal, S.,
735 Davis, K. J., Baier, B. C., and Sweeney, C.: Seasonal Variability in Local Carbon Dioxide Biomass Burning Sources Over Central and Eastern US Using Airborne In Situ Enhancement Ratios, Journal of Geophysical Research: Atmospheres, 126, e2020JD034525, https://doi.org/10.1029/2020JD034525, 2021.

Diskin, G., Podolske, J., Sachse, G., and Slate, T.: Open-path airborne tunable diode laser hygrometer, International Symposium on Optical Science and Technology, SPIE2002.

740 Dunne, E. M., Gordon, H., Kürten, A., Almeida, J., Duplissy, J., Williamson, C., Ortega, I. K., Pringle, K. J., Adamov, A., Baltensperger, U., Barmet, P., Benduhn, F., Bianchi, F., Breitenlechner, M., Clarke, A., Curtius, J., Dommen, J., Donahue, N. M., Ehrhart, S., Flagan, R. C., Franchin, A., Guida, R., Hakala, J., Hansel, A., Heinritzi, M., Jokinen, T., Kangasluoma, J., Kirkby, J., Kulmala, M., Kupc, A., Lawler, M. J., Lehtipalo, K., Makhmutov, V., Mann, G., Mathot, S., Merikanto, J., Miettinen, P., Nenes, A., Onnela, A., Rap, A., Reddington, C. L. S., Riccobono,

745 F., Richards, N. A. D., Rissanen, M. P., Rondo, L., Sarnela, N., Schobesberger, S., Sengupta, K., Simon, M., Sipilä, M., Smith, J. N., Stozhkov, Y., Tomé, A., Tröstl, J., Wagner, P. E., Wimmer, D., Winkler, P. M., Worsnop, D. R., and Carslaw, K. S.: Global atmospheric particle formation from CERN CLOUD measurements, Science, 354, 1119-1124, doi:10.1126/science.aaf2649, 2016.

Fiedler, V., Arnold, F., Ludmann, S., Minikin, A., Hamburger, T., Pirjola, L., Dörnbrack, A., and Schlager, H.:
750 African biomass burning plumes over the Atlantic: aircraft based measurements and implications for H_2SO_4 and HNO_3 mediated smoke particle activation, Atmos. Chem. Phys., 11, 3211-3225, 10.5194/acp-11-3211-2011, 2011.

Gilman, J. B., Lerner, B. M., Kuster, W. C., Goldan, P. D., Warneke, C., Veres, P. R., Roberts, J. M., de Gouw, J. A., Burling, I. R., and Yokelson, R. J.: Biomass burning emissions and potential air quality impacts of volatile
755 organic compounds and other trace gases from fuels common in the US, Atmos. Chem. Phys., 15, 13915-13938, 10.5194/acp-15-13915-2015, 2015.

Gordon, H., Kirkby, J., Baltensperger, U., Bianchi, F., Breitenlechner, M., Curtius, J., Dias, A., Dommen, J., Donahue, N. M., Dunne, E. M., Duplissy, J., Ehrhart, S., Flagan, R. C., Frege, C., Fuchs, C., Hansel, A., Hoyle, C. R., Kulmala, M., Kürten, A., Lehtipalo, K., Makhmutov, V., Molteni, U., Rissanen, M. P., Stozhkov, Y., Tröstl, J.,
760 Tsagkogeorgas, G., Wagner, R., Williamson, C., Wimmer, D., Winkler, P. M., Yan, C., and Carslaw, K. S.: Causes and importance of new particle formation in the present-day and preindustrial atmospheres, Journal of Geophysical Research: Atmospheres, 122, 8739-8760, https://doi.org/10.1002/2017JD026844, 2017.

Hamed, A., Korhonen, H., Sihto, S.-L., Joutsensaari, J., Järvinen, H., Petäjä, T., Arnold, F., Nieminen, T., Kulmala, M., Smith, J. N., Lehtinen, K. E. J., and Laaksonen, A.: The role of relative humidity in continental new particle
765 formation, Journal of Geophysical Research: Atmospheres, 116, https://doi.org/10.1029/2010JD014186, 2011.

Hegg, D. A., Radke, L. F., Hobbs, P. V., and Riggan, P. J.: Ammonia emissions from biomass burning, Geophysical Research Letters, 15, 335-337, https://doi.org/10.1029/GL015i004p00335, 1988.

Helfter, C., Tremper, A. H., Halios, C. H., Kotthaus, S., Bjorkegren, A., Grimmond, C. S. B., Barlow, J. F., and Nemitz, E.: Spatial and temporal variability of urban fluxes of methane, carbon monoxide and carbon dioxide above
770 London, UK, Atmos. Chem. Phys., 16, 10543-10557, 10.5194/acp-16-10543-2016, 2016.

Hennigan, C. J., Westervelt, D. M., Riipinen, I., Engelhart, G. J., Lee, T., Collett Jr., J. L., Pandis, S. N., Adams, P. J., and Robinson, A. L.: New particle formation and growth in biomass burning plumes: An important source of cloud condensation nuclei, Geophysical Research Letters, 39, https://doi.org/10.1029/2012GL050930, 2012.

Hermann, M., Wehner, B., Bischof, O., Han, H. S., Krinke, T., Liu, W., Zerrath, A., and Wiedensohler, A.: Particle
775 counting efficiencies of new TSI condensation particle counters, Journal of Aerosol Science, 38, 674-682, https://doi.org/10.1016/j.jaerosci.2007.05.001, 2007.

Hilario, M. R. A., Cruz, M. T., Cambaliza, M. O. L., Reid, J. S., Xian, P., Simpas, J. B., Lagrosas, N. D., Uy, S. N. Y., Cliff, S., and Zhao, Y.: Investigating size-segregated sources of elemental composition of particulate matter in the South China Sea during the 2011 Vasco cruise, Atmos. Chem. Phys., 20, 1255-1276, 10.5194/acp-20-1255-2020, 2020.

Hilario, M. R. A., Crosbie, E., Shook, M., Reid, J. S., Cambaliza, M. O. L., Simpas, J. B. B., Ziemba, L., DiGangi, J. P., Diskin, G. S., Nguyen, P., Turk, F. J., Winstead, E., Robinson, C. E., Wang, J., Zhang, J., Wang, Y., Yoon, S., Flynn, J., Alvarez, S. L., Behrangi, A., and Sorooshian, A.: Measurement report: Long-range transport patterns into the tropical northwest Pacific during the CAMP2Ex aircraft campaign: chemical composition, size distributions, and the impact of convection, Atmos. Chem. Phys., 21, 3777-3802, 10.5194/acp-21-3777-2021, 2021.

Hodshire, A. L., Ramnarine, E., Akherati, A., Alvarado, M. L., Farmer, D. K., Jathar, S. H., Kreidenweis, S. M., Lonsdale, C. R., Onasch, T. B., Springston, S. R., Wang, J., Wang, Y., Kleinman, L. I., Sedlacek Iii, A. J., and Pierce, J. R.: Dilution impacts on smoke aging: evidence in Biomass Burning Observation Project (BBOP) data, Atmos. Chem. Phys., 21, 6839-6855, 10.5194/acp-21-6839-2021, 2021.

Kazil, J., Lovejoy, E. R., Barth, M. C., and O'Brien, K.: Aerosol nucleation over oceans and the role of galactic cosmic rays, Atmos. Chem. Phys., 6, 4905-4924, 10.5194/acp-6-4905-2006, 2006.

Kerminen, V.-M., Chen, X., Vakkari, V., Petäjä, T., Kulmala, M., and Bianchi, F.: Atmospheric new particle formation and growth: review of field observations, Environmental Research Letters, 13, 103003, 2018.

Khosrawi, F. and Konopka, P.: Enhanced particle formation and growth due to mixing processes in the tropopause region, Atmospheric Environment, 37, 903-910, https://doi.org/10.1016/S1352-2310(02)00976-7, 2003.

Kirkby, J., Curtius, J., Almeida, J., Dunne, E., Duplissy, J., Ehrhart, S., Franchin, A., Gagné, S., Ickes, L., Kürten, A., Kupc, A., Metzger, A., Riccobono, F., Rondo, L., Schobesberger, S., Tsagkogeorgas, G., Wimmer, D., Amorim, A., Bianchi, F., Breitenlechner, M., David, A., Dommen, J., Downard, A., Ehn, M., Flagan, R. C., Haider, S., Hansel, A., Hauser, D., Jud, W., Junninen, H., Kreissl, F., Kvashin, A., Laaksonen, A., Lehtipalo, K., Lima, J., Lovejoy, E. R., Makhmutov, V., Mathot, S., Mikkilä, J., Minginette, P., Mogo, S., Nieminen, T., Onnela, A., Pereira, P., Petäjä, T., Schnitzhofer, R., Seinfeld, J. H., Sipilä, M., Stozhkov, Y., Stratmann, F., Tomé, A., Vanhanen, J., Viisanen, Y., Vrtala, A., Wagner, P. E., Walther, H., Weingartner, E., Wex, H., Winkler, P. M., Carslaw, K. S., Worsnop, D. R., Baltensperger, U., and Kulmala, M.: Role of sulphuric acid, ammonia and galactic cosmic rays in atmospheric aerosol nucleation, Nature, 476, 429-433, 10.1038/nature10343, 2011.

Koehler, K. A., Kreidenweis, S. M., DeMott, P. J., Prenni, A. J., Carrico, C. M., Ervens, B., and Feingold, G.: Water activity and activation diameters from hygroscopicity data - Part II: Application to organic species, Atmos. Chem. Phys., 6, 795-809, 10.5194/acp-6-795-2006, 2006.

Kuang, C., McMurry, P. H., and McCormick, A. V.: Determination of cloud condensation nuclei production from measured new particle formation events, Geophysical Research Letters, 36, https://doi.org/10.1029/2009GL037584, 2009.

Kulmala, M., Petäjä, T., Ehn, M., Thornton, J., Sipilä, M., Worsnop, D. R., and Kerminen, V.-M.: Chemistry of Atmospheric Nucleation: On the Recent Advances on Precursor Characterization and Atmospheric Cluster Composition in Connection with Atmospheric New Particle Formation, Annual Review of Physical Chemistry, 65, 21-37, 10.1146/annurev-physchem-040412-110014, 2014.

815   Kulmala, M., Petäjä, T., Nieminen, T., Sipilä, M., Manninen, H. E., Lehtipalo, K., Dal Maso, M., Aalto, P. P., Junninen, H., Paasonen, P., Riipinen, I., Lehtinen, K. E. J., Laaksonen, A., and Kerminen, V.-M.: Measurement of the nucleation of atmospheric aerosol particles, Nature Protocols, 7, 1651-1667, 10.1038/nprot.2012.091, 2012.

Lawson, P., Gurganus, C., Woods, S., and Bruintjes, R.: Aircraft Observations of Cumulus Microphysics Ranging from the Tropics to Midlatitudes: Implications for a "New" Secondary Ice Process, Journal of the Atmospheric
820   Sciences, 74, 2899-2920, 10.1175/jas-d-17-0033.1, 2017.

Lee, S. H., Young, L.-H., Benson, D. R., Suni, T., Kulmala, M., Junninen, H., Campos, T. L., Rogers, D. C., and Jensen, J. B.: Observations of nighttime new particle formation in the troposphere, Journal of Geophysical Research, 113, 2008.

Lehtipalo, K., Yan, C., Dada, L., Bianchi, F., Xiao, M., Wagner, R., Stolzenburg, D., Ahonen, L. R., Amorim, A.,
825   Baccarini, A., Bauer, P. S., Baumgartner, B., Bergen, A., Bernhammer, A.-K., Breitenlechner, M., Brilke, S., Buchholz, A., Mazon, S. B., Chen, D., Chen, X., Dias, A., Dommen, J., Draper, D. C., Duplissy, J., Ehn, M., Finkenzeller, H., Fischer, L., Frege, C., Fuchs, C., Garmash, O., Gordon, H., Hakala, J., He, X., Heikkinen, L., Heinritzi, M., Helm, J. C., Hofbauer, V., Hoyle, C. R., Jokinen, T., Kangasluoma, J., Kerminen, V.-M., Kim, C., Kirkby, J., Kontkanen, J., Kürten, A., Lawler, M. J., Mai, H., Mathot, S., Mauldin, R. L., Molteni, U., Nichman, L.,
830   Nie, W., Nieminen, T., Ojdanic, A., Onnela, A., Passananti, M., Petäjä, T., Piel, F., Pospisilova, V., Quéléver, L. L. J., Rissanen, M. P., Rose, C., Sarnela, N., Schallhart, S., Schuchmann, S., Sengupta, K., Simon, M., Sipilä, M., Tauber, C., Tomé, A., Tröstl, J., Väisänen, O., Vogel, A. L., Volkamer, R., Wagner, A. C., Wang, M., Weitz, L., Wimmer, D., Ye, P., Ylisirniö, A., Zha, Q., Carslaw, K. S., Curtius, J., Donahue, N. M., Flagan, R. C., Hansel, A., Riipinen, I., Virtanen, A., Winkler, P. M., Baltensperger, U., Kulmala, M., and Worsnop, D. R.: Multicomponent
835   new particle formation from sulfuric acid, ammonia, and biogenic vapors, Science Advances, 4, eaau5363, doi:10.1126/sciadv.aau5363, 2018.

Lloyd, S.: Least squares quantization in PCM, IEEE Transactions on Information Theory, 28, 129-137, 10.1109/TIT.1982.1056489, 1982.

Meinardi, S., Simpson, I. J., Blake, N. J., Blake, D. R., and Rowland, F. S.: Dimethyl disulfide (DMDS) and
840   dimethyl sulfide (DMS) emissions from biomass burning in Australia, Geophysical Research Letters, 30, https://doi.org/10.1029/2003GL016967, 2003.

Nara, H., Tanimoto, H., Tohjima, Y., Mukai, H., Nojiri, Y., and Machida, T.: Emission factors of CO2, CO and CH4 from Sumatran peatland fires in 2013 based on shipboard measurements, Tellus B Chem Phys Meteorol, 69, 10.1080/16000889.2017.1399047, 2017.

845   Nilsson, E. D. and Kulmala, M.: The potential for atmospheric mixing processes to enhance the binary nucleation rate, Journal of Geophysical Research: Atmospheres, 103, 1381-1389, https://doi.org/10.1029/97JD02629, 1998.

Nilsson, E. D., Rannik, Ü., Kumala, M., Buzorius, G., and O'dowd, C. D.: Effects of continental boundary layer evolution, convection, turbulence and entrainment, on aerosol formation, Tellus B: Chemical and Physical Meteorology, 53, 441-461, 10.3402/tellusb.v53i4.16617, 2001.

850   Norgren, M. S., Wood, J., Schmidt, K. S., van Diedenhoven, B., Stamnes, S. A., Ziemba, L. D., Crosbie, E. C., Shook, M. A., Kittelman, A. S., LeBlanc, S. E., Broccardo, S., Freitag, S., and Reid, J. S.: Above-aircraft cirrus cloud and aerosol optical depth from hyperspectral irradiances measured by a total-diffuse radiometer, Atmos. Meas. Tech., 15, 1373-1394, 10.5194/amt-15-1373-2022, 2022.

Perry, K. D. and Hobbs, P. V.: Further evidence for particle nucleation in clear air adjacent to marine cumulus
855   clouds, Journal of Geophysical Research: Atmospheres, 99, 22803-22818, https://doi.org/10.1029/94JD01926, 1994.

Petters, M. D. and Kreidenweis, S. M.: A single parameter representation of hygroscopic growth and cloud condensation nucleus activity, Atmos. Chem. Phys., 7, 1961-1971, 10.5194/acp-7-1961-2007, 2007.

Pirjola, L., O'Dowd, C. D., Brooks, I. M., and Kulmala, M.: Can new particle formation occur in the clean marine boundary layer?, Journal of Geophysical Research: Atmospheres, 105, 26531-26546,
860   https://doi.org/10.1029/2000JD900310, 2000.

Podolske, J. R., Sachse, G. W., and Diskin, G. S.: Calibration and data retrieval algorithms for the NASA Langley/Ames Diode Laser Hygrometer for the NASA transport and chemical evolution over the pacific (TRACE-P) mission, Journal of Geophysical Research: Atmospheres, 108, 2003.

Reid, J. S., Posselt, D. J., Kaku, K., Holz, R. A., Chen, G., Eloranta, E. W., Kuehn, R. E., Woods, S., Zhang, J.,
865   Anderson, B., Bui, T. P., Diskin, G. S., Minnis, P., Newchurch, M. J., Tanelli, S., Trepte, C. R., Thornhill, K. L., and Ziemba, L. D.: Observations and hypotheses related to low to middle free tropospheric aerosol, water vapor and altocumulus cloud layers within convective weather regimes: a SEAC4RS case study, Atmos. Chem. Phys., 19, 11413-11442, 10.5194/acp-19-11413-2019, 2019.

Reid, J. S., Lagrosas, N. D., Jonsson, H. H., Reid, E. A., Atwood, S. A., Boyd, T. J., Ghate, V. P., Xian, P., Posselt,
870   D. J., Simpas, J. B., Uy, S. N., Zaiger, K., Blake, D. R., Bucholtz, A., Campbell, J. R., Chew, B. N., Cliff, S. S., Holben, B. N., Holz, R. E., Hyer, E. J., Kreidenweis, S. M., Kuciauskas, A. P., Lolli, S., Oo, M., Perry, K. D., Salinas, S. V., Sessions, W. R., Smirnov, A., Walker, A. L., Wang, Q., Yu, L., Zhang, J., and Zhao, Y.: Aerosol meteorology of Maritime Continent for the 2012 7SEAS southwest monsoon intensive study – Part 2: Philippine receptor observations of fine-scale aerosol behavior, Atmos. Chem. Phys., 16, 14057-14078, 10.5194/acp-16-14057-
875   2016, 2016.

Reid, J. S., Maring, H. B., Narisma, G. T., van den Heever, S., Di Girolamo, L., Ferrare, R., Lawson, P., Mace, G. G., Simpas, J. B., Tanelli, S., Ziemba, L., van Diedenhoven, B., Bruintjes, R., Bucholtz, A., Cairns, B., Cambaliza,

M. O., Chen, G., Diskin, G. S., Flynn, J. H., Hostetler, C. A., Holz, R. E., Lang, T. J., Schmidt, K. S., Smith, G., Sorooshian, A., Thompson, E. J., Thornhill, K. L., Trepte, C., Wang, J., Woods, S., Yoon, S., Alexandrov, M.,

880   Alvarez, S., Amiot, C. G., Bennett, J. R., Brooks, M., Burton, S. P., Cayanan, E., Chen, H., Collow, A., Crosbie, E., DaSilva, A., DiGangi, J. P., Flagg, D. D., Freeman, S. W., Fu, D., Fukada, E., Hilario, M. R. A., Hong, Y., Hristova-Veleva, S. M., Kuehn, R., Kowch, R. S., Leung, G. R., Loveridge, J., Meyer, K., Miller, R. M., Montes, M. J., Moum, J. N., Nenes, T., Nesbitt, S. W., Norgren, M., Nowottnick, E. P., Rauber, R. M., Reid, E. A., Rutledge, S., Schlosser, J. S., Sekiyama, T. T., Shook, M. A., Sokolowsky, G. A., Stamnes, S. A., Tanaka, T. Y., Wasilewski, A.,

885   Xian, P., Xiao, Q., Xu, Z., and Zavaleta, J.: The coupling between tropical meteorology, aerosol lifecycle, convection, and radiation, during the Cloud, Aerosol and Monsoon Processes Philippines Experiment (CAMP2Ex), Bulletin of the American Meteorological Society, https://doi.org/10.1175/BAMS-D-21-0285.1, 2023.

Rousseeuw, P. J.: Silhouettes: A graphical aid to the interpretation and validation of cluster analysis, Journal of Computational and Applied Mathematics, 20, 53-65, https://doi.org/10.1016/0377-0427(87)90125-7, 1987.

890   Schmidt, K. S., Wendisch, M., and Kindel, B.: Airborne Solar Radiation Sensors, in: Springer Handbook of Atmospheric Measurements, edited by: Foken, T., Springer International Publishing, Cham, 1131-1150, 10.1007/978-3-030-52171-4_40, 2021.

Shang, D., Hu, M., Zheng, J., Qin, Y., Du, Z., Li, M., Fang, J., Peng, J., Wu, Y., Lu, S., and Guo, S.: Particle number size distribution and new particle formation under the influence of biomass burning at a high altitude

895   background site at Mt. Yulong (3410 m), China, Atmos. Chem. Phys., 18, 15687-15703, 10.5194/acp-18-15687-2018, 2018.

Spracklen, D. V., Carslaw, K. S., Pöschl, U., Rap, A., and Forster, P. M.: Global cloud condensation nuclei influenced by carbonaceous combustion aerosol, Atmos. Chem. Phys., 11, 9067-9087, 10.5194/acp-11-9067-2011, 2011.

900   Stolzenburg, D., Fischer, L., Vogel, A. L., Heinritzi, M., Schervish, M., Simon, M., Wagner, A. C., Dada, L., Ahonen, L. R., Amorim, A., Baccarini, A., Bauer, P. S., Baumgartner, B., Bergen, A., Bianchi, F., Breitenlechner, M., Brilke, S., Buenrostro Mazon, S., Chen, D., Dias, A., Draper, D. C., Duplissy, J., El Haddad, I., Finkenzeller, H., Frege, C., Fuchs, C., Garmash, O., Gordon, H., He, X., Helm, J., Hofbauer, V., Hoyle, C. R., Kim, C., Kirkby, J., Kontkanen, J., Kürten, A., Lampilahti, J., Lawler, M., Lehtipalo, K., Leiminger, M., Mai, H., Mathot, S., Mentler,

905   B., Molteni, U., Nie, W., Nieminen, T., Nowak, J. B., Ojdanic, A., Onnela, A., Passananti, M., Petäjä, T., Quéléver, L. L. J., Rissanen, M. P., Sarnela, N., Schallhart, S., Tauber, C., Tomé, A., Wagner, R., Wang, M., Weitz, L., Wimmer, D., Xiao, M., Yan, C., Ye, P., Zha, Q., Baltensperger, U., Curtius, J., Dommen, J., Flagan, R. C., Kulmala, M., Smith, J. N., Worsnop, D. R., Hansel, A., Donahue, N. M., and Winkler, P. M.: Rapid growth of organic aerosol nanoparticles over a wide tropospheric temperature range, Proceedings of the National Academy of Sciences, 115,

910   9122-9127, doi:10.1073/pnas.1807604115, 2018.

Syakur, M. A., Khotimah, B. K., Rochman, E. M. S., and Satoto, B. D.: Integration K-Means Clustering Method and Elbow Method For Identification of The Best Customer Profile Cluster, IOP Conference Series: Materials Science and Engineering, 336, 012017, 10.1088/1757-899x/336/1/012017, 2018.

Twohy, C. H., Clement, C. F., Gandrud, B. W., Weinheimer, A. J., Campos, T. L., Baumgardner, D., Brune, W. H., Faloona, I., Sachse, G. W., Vay, S. A., and Tan, D.: Deep convection as a source of new particles in the midlatitude upper troposphere, Journal of Geophysical Research: Atmospheres, 107, AAC 6-1-AAC 6-10, https://doi.org/10.1029/2001JD000323, 2002.

Uhrner, U., Zallinger, M., von Löwis, S., Vehkamäki, H., Wehner, B., Stratmann, F., and Wiedensohler, A.: Volatile Nanoparticle Formation and Growth within a Diluting Diesel Car Exhaust, Journal of the Air & Waste Management Association, 61, 399-408, 10.3155/1047-3289.61.4.399, 2011.

Vakkari, V., Beukes, J. P., Dal Maso, M., Aurela, M., Josipovic, M., and van Zyl, P. G.: Major secondary aerosol formation in southern African open biomass burning plumes, Nature Geoscience, 11, 580-583, 10.1038/s41561-018-0170-0, 2018.

Vehkamäki, H., Kulmala, M., Napari, I., Lehtinen, K. E. J., Timmreck, C., Noppel, M., and Laaksonen, A.: An improved parameterization for sulfuric acid–water nucleation rates for tropospheric and stratospheric conditions, Journal of Geophysical Research: Atmospheres, 107, AAC 3-1-AAC 3-10, https://doi.org/10.1029/2002JD002184, 2002.

Wang, J., Pikridas, M., Spielman, S. R., and Pinterich, T.: A fast integrated mobility spectrometer for rapid measurement of sub-micrometer aerosol size distribution, Part I: Design and model evaluation, Journal of Aerosol Science, 108, 44-55, 2017a.

Wang, J., Pikridas, M., Pinterich, T., Spielman, S. R., Tsang, T., McMahon, A., and Smith, S.: A Fast Integrated Mobility Spectrometer for rapid measurement of sub-micrometer aerosol size distribution, Part II: Experimental characterization, Journal of Aerosol Science, 113, 119-129, https://doi.org/10.1016/j.jaerosci.2017.05.001, 2017b.

Wang, Y., Pinterich, T., and Wang, J.: Rapid measurement of sub-micrometer aerosol size distribution using a fast integrated mobility spectrometer, Journal of Aerosol Science, 121, 12-20, https://doi.org/10.1016/j.jaerosci.2018.03.006, 2018.

Wehner, B., Uhrner, U., von Löwis, S., Zallinger, M., and Wiedensohler, A.: Aerosol number size distributions within the exhaust plume of a diesel and a gasoline passenger car under on-road conditions and determination of emission factors, Atmospheric Environment, 43, 1235-1245, https://doi.org/10.1016/j.atmosenv.2008.11.023, 2009.

Wehner, B., Werner, F., Ditas, F., Shaw, R. A., Kulmala, M., and Siebert, H.: Observations of new particle formation in enhanced UV irradiance zones near cumulus clouds, Atmos. Chem. Phys., 15, 11701-11711, 10.5194/acp-15-11701-2015, 2015.

Wehner, B., Siebert, H., Ansmann, A., Ditas, F., Seifert, P., Stratmann, F., Wiedensohler, A., Apituley, A., Shaw, R. A., Manninen, H. E., and Kulmala, M.: Observations of turbulence-induced new particle formation in the residual layer, Atmos. Chem. Phys., 10, 4319-4330, 10.5194/acp-10-4319-2010, 2010.

Williamson, C. J., Kupc, A., Axisa, D., Bilsback, K. R., Bui, T., Campuzano-Jost, P., Dollner, M., Froyd, K. D., Hodshire, A. L., Jimenez, J. L., Kodros, J. K., Luo, G., Murphy, D. M., Nault, B. A., Ray, E. A., Weinzierl, B., Wilson, J. C., Yu, F., Yu, P., Pierce, J. R., and Brock, C. A.: A large source of cloud condensation nuclei from new particle formation in the tropics, Nature, 574, 399-403, 10.1038/s41586-019-1638-9, 2019.

Worden, J. R., Bloom, A. A., Pandey, S., Jiang, Z., Worden, H. M., Walker, T. W., Houweling, S., and Röckmann, T.: Reduced biomass burning emissions reconcile conflicting estimates of the post-2006 atmospheric methane budget, Nature Communications, 8, 2227, 10.1038/s41467-017-02246-0, 2017.

Xian, P., Reid, J. S., Atwood, S. A., Johnson, R. S., Hyer, E. J., Westphal, D. L., and Sessions, W.: Smoke aerosol transport patterns over the Maritime Continent, Atmospheric Research, 122, 469-485, https://doi.org/10.1016/j.atmosres.2012.05.006, 2013.

Yao, L., Garmash, O., Bianchi, F., Zheng, J., Yan, C., Kontkanen, J., Junninen, H., Mazon, S. B., Ehn, M., Paasonen, P., Sipilä, M., Wang, M., Wang, X., Xiao, S., Chen, H., Lu, Y., Zhang, B., Wang, D., Fu, Q., Geng, F., Li, L., Wang, H., Qiao, L., Yang, X., Chen, J., Kerminen, V.-M., Petäjä, T., Worsnop, D. R., Kulmala, M., and Wang, L.: Atmospheric new particle formation from sulfuric acid and amines in a Chinese megacity, Science, 361, 278-281, doi:10.1126/science.aao4839, 2018.

Yee, L. D., Kautzman, K. E., Loza, C. L., Schilling, K. A., Coggon, M. M., Chhabra, P. S., Chan, M. N., Chan, A. W. H., Hersey, S. P., Crounse, J. D., Wennberg, P. O., Flagan, R. C., and Seinfeld, J. H.: Secondary organic aerosol formation from biomass burning intermediates: phenol and methoxyphenols, Atmos. Chem. Phys., 13, 8019-8043, 10.5194/acp-13-8019-2013, 2013.

Zhang, R., Khalizov, A., Wang, L., Hu, M., and Xu, W.: Nucleation and Growth of Nanoparticles in the Atmosphere, Chemical Reviews, 112, 1957-2011, 10.1021/cr2001756, 2012.

Zheng, G., Wang, Y., Wood, R., Jensen, M. P., Kuang, C., McCoy, I. L., Matthews, A., Mei, F., Tomlinson, J. M., and Shilling, J. E.: New particle formation in the remote marine boundary layer, Nature communications, 12, 1-10, 2021.

Zhu, Y., Sabaliauskas, K., Liu, X., Meng, H., Gao, H., Jeong, C.-H., Evans, G. J., and Yao, X.: Comparative analysis of new particle formation events in less and severely polluted urban atmosphere, Atmospheric Environment, 98, 655-664, https://doi.org/10.1016/j.atmosenv.2014.09.043, 2014.

975